Studies of Cytokinesis in Fission Yeast Protoplast

by

Tzer Chyn Lim

A thesis submitted for the degree of

Doctor of Philosophy in Medical Sciences

WMS, University of Warwick

January 2020

CONTENTS

LIST OF FIGURES

LIST OF TABLES

ACKNOWLEDGEMENTS

First of all, I would like to express my deepest gratitude to my supervisors, Professor Mohan K. Balasubramanian and Professor Jonathan Millar for honoring me the opportunity to do embark on the journey of PhD. I thank them for the invaluable guidance, comments and suggestions throughout the years which allow me to arrive at this point of the course.

My completion of this course could not have been possible without the guidance and help of all my present and past laboratory colleagues. I would like to sincerely thank these wonderful people for the tremendous amount of help while I work on the research projects. There are a few colleagues whom I would like to specially mention, they are:

- Dr Ting Gang Chew, as he gave me the earliest guidance when I joined the laboratory. My projects would not have been completed without his many words of opinion and guidance in technically.
- Dr Jun Qi Huang, as he passed to me much of his experience of super resolution microscopy and image processing techniques. These skills were later translated into many important results in my projects.
- Dr Anton Kamnev, for the proper instruction of using advanced microscope. He also contributed to the curvature measurement of spheroplasts and rings.
- Dr Tomoyuki Hatano, for the guidance on a few projects I was involved in. Not to forget his contribution to the *in-vitro* treatment of actin filaments. He also helped out with our communication with our collaborator, Professor Masako Osumi.

- Dr Saravanan Palani and Paola Zambon for the protocols and advice for my experiments.

Profound thanks to our collaborator, Professor Masako Osumi for looking into the extracellular matrix of spheroplasts.

Last but not least, my deepest thanks to my family and friends for their endless support and care while I am pursuing my degree abroad. They are my pillar of strength who are encouraging and motivating me.

DECLARATIONS

I hereby declare that this thesis titled “Studies of Cytokinesis in Fission Yeast Protoplasts” is my own work and solely written by myself. The work presented in this thesis is my own, except in instances involving collaborative work which is mentioned in the figure caption or main text. This thesis has not been submitted for a higher degree to any other university or institution.

Tzer Chyn Lim,

15th January 2020

ABSTRACT

In many organisms, cytokinesis is facilitated by an actomyosin-based contractile ring. Positioning of the ring requires close coordination of positive and negative-signaling cues, coupled with cell geometry and nuclear position. The fission yeast *S. pombe* relies on these spatial cues to accomplish stable ring assembly. After proper positioning of the actomyosin ring, the ring contracts to drive membrane invagination, cell wall assembly, and to complete cell separation into two daughter cells. Although this model organism has its specificities, knowledge of the basic mechanisms and roles of actomyosin ring could be useful to understand similar mechanisms in other organisms.

We were curious about how a fission yeast maintain a robust cell division machinery, if majority of cell wall is absent. In cylindrical fission yeast cells, coordination of actomyosin ring positioning is facilitated by a positive spatial cue, *mid1* and a negative spatial cue, the tip-complex. In spherical protoplast of fission yeast, we observed mislocalized spatial cues, while the actomyosin ring consistently assemble at the equatorial region. Although removal of *mid1 and* the tip-complex in cylindrical cells caused the actomyosin ring to assemble along the long axis, it did not hinder the equatorial assembly of actomyosin ring in the spherical protoplasts. We found that actin filaments played a role as major determinant of positioning actomyosin ring in the absence of spatial cues.

Given the spheroplasts are capable of forming an equatorial ring, we then asked whether the actomyosin ring is capable of contracting and bring about cytofission. The *cps1* mutant, a cell wall mutant lacking β-glucan synthase function is unable to overcome its turgor pressure and undergo actomyosin ring contraction. We found that by generating protoplasts, cytofission (which we define as a process that separates the cytosol into two membrane-bound entities) took place and the protoplast was divided into two entities. We report that this event does not require α-glucan (another component of cell wall), exoglucanases to facilitate breakdown residual septum, and ESCRT proteins. The actomyosin ring is however essential for cytofission.

LIST OF ABBREVIATION

2-DG	-	2-deoxy-D-glucose
AM	-	Actomyosin ring
atb2	-	Tubulin alpha 2
ATP	-	Adenosine triphosphate
C. elegans	-	*Caenorhabditis elegans*
CAR	-	Contractile actomyosin ring
CW	-	Calcofluor white
DAPI	-	4', 6-diamidino-2-phenylindole
DMSO	-	Dimethyl sulfoxide
EGFP	-	Enhanced green fluorescent protein
ELN	-	Exocet Low Nitrogen
EMMA	-	Edinburgh Minimal Medium
GAP	-	GTPase-activating proteins
GEF	-	Guanine nucleotide exchange factors
GFP	-	Green fluorescent protein
GTP	-	Guanosine-5'-triphosphate
hph	-	Hygromycin B
kan	-	Kanamycin A
Lat-A	-	Latrunculin A
MEN	-	Mitotic exit network
MP-GAP	-	M phase GAP
MRLC	-	Myosin regulatory light chain
nat	-	Nourseothricin
PAK	-	p21-activated kinases
PBS	-	Phosphate-buffered saline
PFA	-	Paraformaldehyde
R	-	Ring diameter
ROCK	-	*Rho*-associated protein *kinase*
RPM	-	Revolution per minute

S	-	Spheroplast diameter
S. pombe	-	*Schizosaccharomyces pombe*
SD	-	Standard deviation
SIN	-	Septation initiation network
TIRF	-	Total internal reflection fluorescence
YES	-	Yeast Extract with Supplements

1. INTRODUCTION

1.1 CYTOKINESIS

Cytokinesis is the final stage of cell division, in which a parental cell undergoes physical separation of the cytoplasmic contents into two identical daughter cells. In many eukaryotes, this event requires extensive finely regulated cell processes such as the specification of division plane, assembly of an actomyosin-based contractile ring, and ring constriction. Given the complexity and significance of cytokinesis, a cell produces and utilizes a vast variety of proteins to enable successful cell division. In *S. pombe*, more than 130 genes and proteins are known to involve in functions of contractile actomyosin ring [1, 2].

1.1.1 Cytokinesis in bacterial cells

Bacteria accomplish cytokinesis by the multicomponent divisome machinery. The divisome machinery assembles at midcell to facilitate the contraction of the multilayer cell envelope. The cytokinetic ring in bacterial cells was first described as FtsZ, known as the “Z ring”, which is part of the divisome machinery and is present in many eukaryotes [3, 4]. FtsZ, a tubulin-like protein forms the Z ring at midcell, is functionally analogous to eukaryotic actomyosin ring – it contracts to drive membrane invagination during cytokinesis [3, 5-7]. However, later studies implicated that FtsZ was a homolog of tubulin, due to the presence of a tubulin signature amino acid sequence and the fact that FtsZ binds and hydrolyzes GTP [8-10]. FtsA and MreB are both regarded as essential actin homologs of *E. coli* and other bacteria, as they display clear structural homologs of actin [11-13]. FtsA is required

for constriction of the Z ring and recruitment of later divisome proteins [14, 15]. In cells, MreB exists as mobile patches and filaments on the cytoplasmic membrane, and is often detected at mid cell [16]. Fenton e*t al.* showed that E. coli MreB indeed interacts with FtsZ, and this interaction is also required for Z ring constriction [17]. In *Chlamydia*, MreB plays a crucial role to function as FtsZ ring [18, 19].

The localization of FtsZ is reported to be dependent of two inhibitory mechanisms. A bacteria cell that is about to divide has two nucleoids containing bacterial genome. The localization of the two nucleoids inhibits localization of the Z ring in their vicinity, hence leaving spaces available for Z ring assembly at either midcell or cell pole [6, 20]. In *E. coli*, the *min* proteins are MinC, MinD and MinE. They blocks Z ring polymerization from the cell poles. Specifically, MinC and MinD negatively regulate FtsZ ring assembly [21]. However, more recent evidence suggest that Min proteins localize to midcell to prevent multiple Z ring formation there, and establish a new bipolar gradient in daughter cells [22, 23]. The Z ring is formed by bidirectional polymerization from one nucleation site at midcell [24]. Subsequently other proteins were recruited by Z ring to carry out cytokinesis [25, 26].

The Z ring contraction has been described with several models. It has been proposed that short filaments of the ring slide in relative to each other to reduce the circumference of the ring[27]. Others have proposed the Z ring contract by depolymerization at its anchor site, losing its FtsZ subunits [5]. In another model, the Z ring is described to be composed of straight protofilaments that can be hydrolyzed by Guanosine-5'-triphosphate (GTP) to curve [3, 28]. As the protofilaments are assembled, the collective force of curvature is achieved to overcome curvature of the cell and initiate ring contraction [29, 30]. Cell separation

after Z ring contraction is aided by the ingrowth of peptidoglycan cell wall [5].

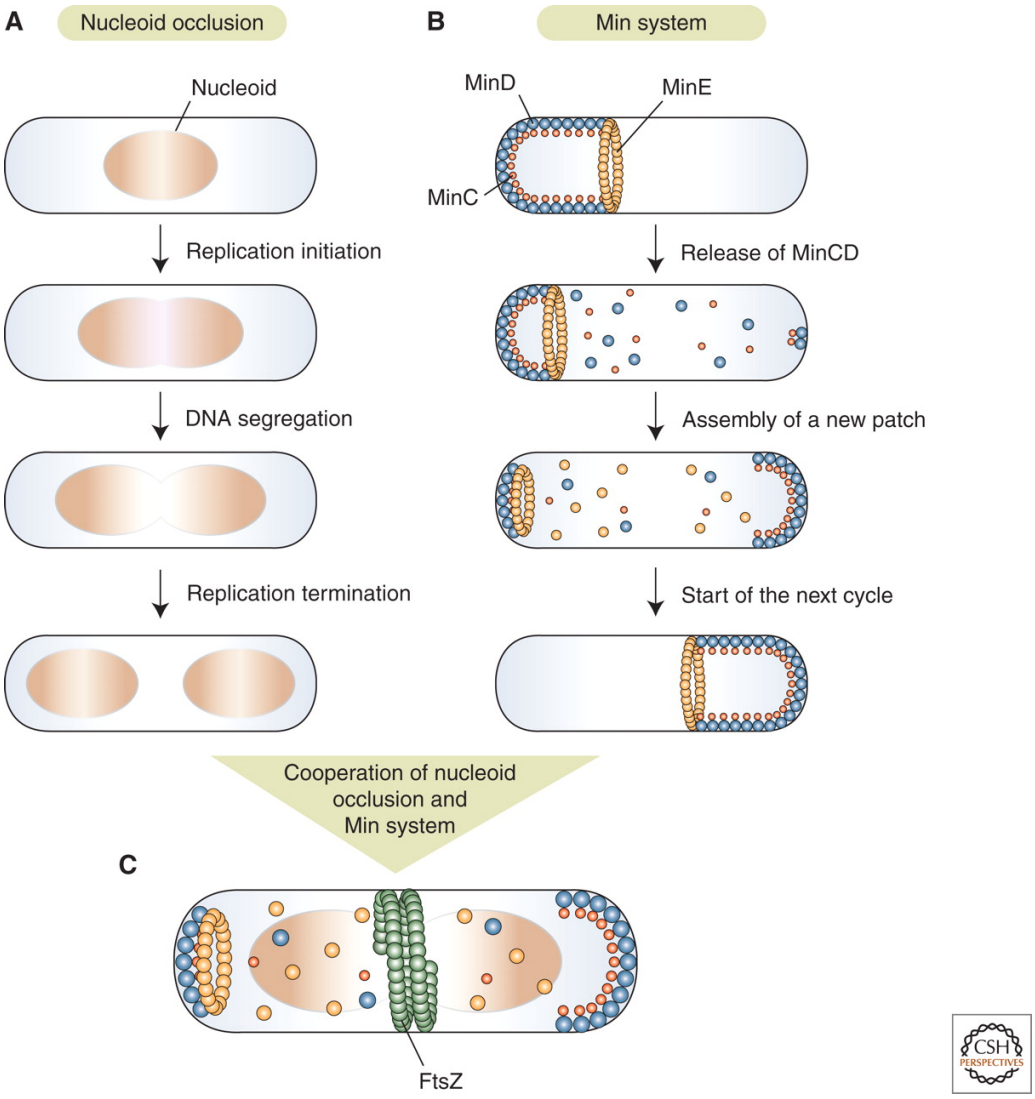

Figure 1.1 Bacterial cell FtsZ ring placement.

(A) Temporal and spatial regulation of cell division by nucleoid occlusion. Two nucleoids move apart during couse of chromosome replication and segregation, allowing nucleoid occlusion protein SlmA to localize at midcell for FtsZ ring to assemble.

(B) Inhibition of polar cell-division events by the *min* system. MinCD forms cap-like later at cell tip to prevent FtsZ ring formation. MinE gradually displaces MinCD from the cell pole. Free MinC and MinD reassemble at the opposite cell pole to restart the cell cycle.
(C) Nucleoid occlusion mechanism and the *min* system cooperate to ensure FtsZ ring formation at midcell. (Source: Illustration taken from Marthin Thanbichler, CSH Perspectives, 2010)

1.1.2 Cytokinesis in animal cells

The formation of contractile ring in animal cells for cytokinesis is governed by active Rho-GTP. Rho-GTP activates Rho-associated protein kinase (ROCK) to phosphorylate the myosin regulatory light chain (MRLC) as well as activating the formins to assemble actin filaments [31-37]. The actomyosin ring of animal cells positioning is a result of myosin II's forces on actin filaments. Myosin motors at the equatorial band interact with actin filaments to form the contractile ring. Myosin motor activity requires phosphorylation of its light chains [38]. Activation of myosin motor generates a tension to slide actin filaments for ring contraction [39]. Genetic perturbations of myosin II and microinjection of anti-myosin II antibodies have been shown to prevent cleavage furrow ingression [39-43].

1.2 Fission yeast *S. pombe* as model organism to study cytokinesis

Our current grasp of knowledge about cell division is largely obtained from studying simple model system, such as the fission yeast *Schizosaccharomyces pombe* (*S. pombe*). *S. pombe* is a rod shaped unicellular organism that grows by linear extension at its tips while cell width remains unchanged. Closed mitosis takes place, and they divide via binary fission using the contractile actomyosin ring (CAR). It is hence

an excellent model organism for studying cytokinesis, because actomyosin ring is widely conserved among eukaryotes. In addition, various experimental approaches and resources are available and can be conveniently applied on the *S. pombe*. Fission yeast genome is small and fully sequenced – about 15 million base pairs on three chromosomes. Experimental studies of gene function are greatly simplified in haploid cells. Coincidentally, fission yeast proliferates as haploids and do not mate unless deprived of nitrogen. Therefore it is easy to isolate and characterize mutations in yeast, as researchers avoid the complication of analyzing the gene in the presence of a second copy of the gene.

1.3 DIVISION SITE PLACEMENT

1.3.1 Introduction

Division site selection is a critical process in cytokinesis because it ensures proper segregation of chromosomes between daughter cells [44]. Failure in controlling division plane orientation can result in genomic instability and lead to diseases such as cancer and blood disorders [45].

In 1884, German zoologist and Professor Oscar Hertwig studied the divisions of frog eggs. A frog egg is round in shape and the first division occurs in random orientation. With two parallel planes, Hertwig compressed a frog egg from round to elongated shape. He observed that the frog eggs acquired a pattern of dividing along the long axis. He then introduced Hertwig's rule or 'long axis rule'. The rule proposed that a cell divides along its long axis due to default orientation of spindle apparatus according to cell shape (Hertwig O, 1884). This theory is supported by recent studies in animal systems. Columnar cells in Xenopus blastomeres tend to divide perpendicularly. In isolation, these cells round up and perpendicular division decreased from 26% to 16% [46]. As every point on the surface of a sphere is equidistant from its centre, the result could suggest a randomized division site placement in a spherical cell.

1.3.2 Division site placement in animal cells

Rappaport (1961) proposed that spindle microtubules were key to determining the cleavage plane positioning in animal cells. After anaphase onset, mitotic spindles rearrange into an array of antiparallel

between the two centrosomal asters, known as the central spindle [47, 48]. The spindle positioning information is transmitted to the cell cortex and that translate into precise division plane positioning.

The small GTPase RhoA has been reported to control contractile ring assembly and constriction by activating two signalling pathways [36, 49]. RhoA stimulates profilin-mediated actin polymerization by binding the diaphanous members of formin-homology proteins. In addition, RhoA/ROCK interaction also phosphorylates the myosin regulatory light chain (MRLC) at Ser19 to increase myosin ATPase activity, thereby promoting myosin contractility [48]. Hence, it is believed that the localization of RhoA around the equatorial cortex is the key element in cleavage furrow formation and ingression [47, 50].

Recent work in *Caenorhabditis elegans* (*C. elegans*) embryo suggests that RhoA also serve as an inhibitor to equatorial assembly of contractile ring proteins accumulation on the polar cortex. During mitosis, RhoA is activated by the Rho-GEF (ECT-2) and inactivated by MP-GAP (known as RGA3/4 in *C. elegans*) [51-53]. When cells are depleted of myosin and RGA3/4, equatorial anillin were slower to accumulate while level of anillin at polar cortex decreased after anaphase onset.

Besides RhoA, Aurora A kinase and its activator, TPXL-1 are reported to play a role in clearing anillin and F-actin from polar cortex, thereby inhibiting contractile ring assembly. Aurora A and TPXL-1 localize to the centrosome and astral microtubules [54, 55]. Depletion of TPXL-1 resulted in shorter spindles due to reduced length of kinetochore microtubules [56]. Meanwhile, anillin and F-actin were not cleared from polar cortex. Restoration of centrosomal asters to a near-normal position did not restore the clearing action at polar cortex [57].

1.3.3 Division site placement in budding yeast

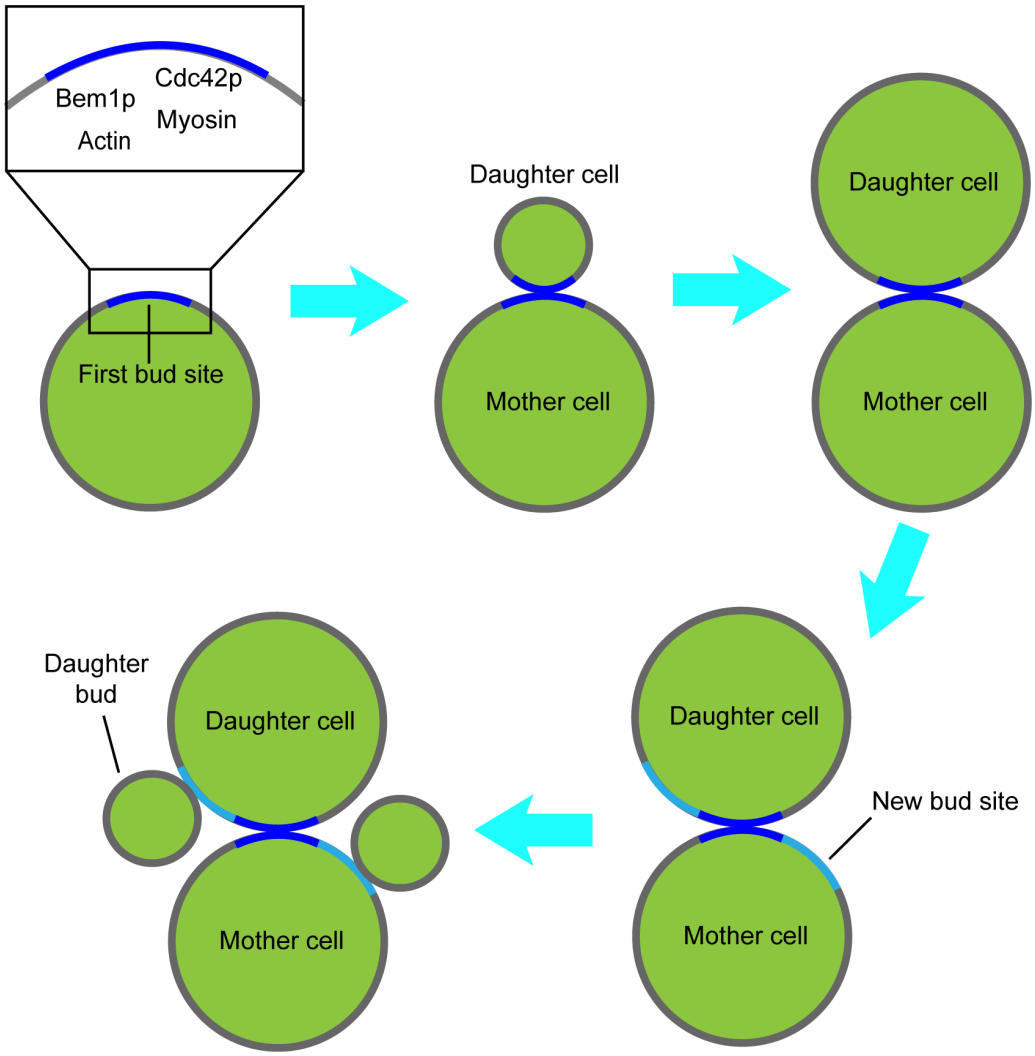

Figure 1.2 Budding yeast division site placement.

Bem1p, Cdc42p, actin and myosin accumulate at bus site and form a cortical ring. Separation of mother and daughter cell leaves behind a bud scar. New bud site will form next to the bud scar. (Illustration modified from Sanders and Field, Current Biology, 1995)

In budding yeast, the contractile ring placement relies on both positive and negative feedback from various proteins near the site of previous cytokinesis (bud scar). Active GTP-cdc42 binds to the plasma membrane with its C-terminal prenyl modification [58]. It interacts with

p21-activated kinases (PAK) that is associated with the scaffold Bem1, Bem1 in turn binds Cdc24, the GEF for Cdc42 [59-64]. The GEF activates other nearby Cdc42 to amplify the process. The negative regulation originates from a Cdc42 GAP called Rga1 remains at the previous cleavage site to block Cdc42 accumulation. Transmembrane proteins positioned next to the bud scar activates a GTPase, Rsr1 that activates Cdc24 GEF to activate Cdc42. Activated Cdc42 recruits the precursors of the contractile ring [58].

Cdc42 recruits five mitotic septins, namely Cdc3, Cdc10, Cdc12, Cdc11 and Shs1 in late G1. They are thought to form octameric complexes with Cdc3, Cdc10 and Cdc12 as the core while Cdc11 and Shs1 are replaceable by each other [65, 66]. Mediated by Cdc42, the septins accumulate at the bud site and form a cortical ring [67]. They expand into an hourglass at the border between the mother cell and bud [68]. When the cell enters cytokinesis, the mitotic exit network (MEN) signals the septin structure to collapse into two cortical rings, sandwiching the actomyosin ring [68]. Studies have shown that the mitotic septins are essential for actomyosin ring assembly in budding yeast, as Myo1 fails to assemble at division site in septin mutants which leads to failure of actin assembly [69, 70].

1.3.4 Division plane placement in fission yeast

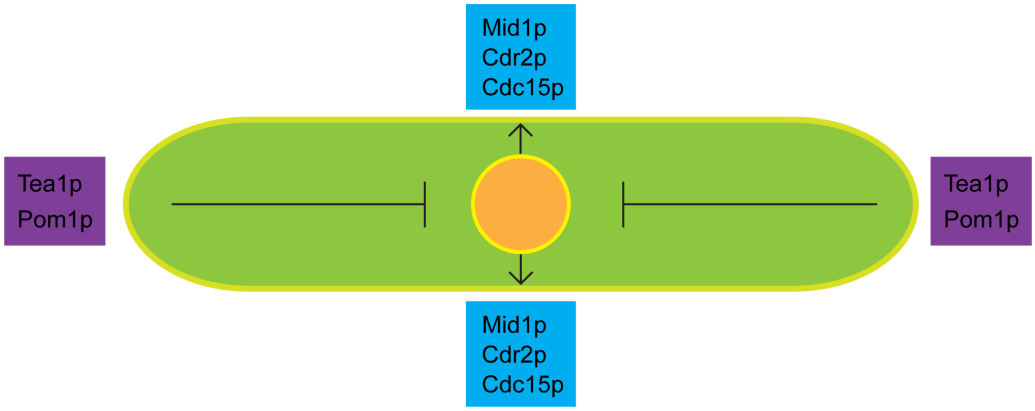

Figure 1.3 The spatial cues that contribute to the positioning of division plane.

Mid1p acts as positive cue. Mid1p localizes at the cortex adjacent to nucleus and recruit ring components there. Tip complex (Tea1p, Pom1p) acts as a negative cue, by phosphorylating the F-BAR protein Cdc15p so that the ring slides from cell tip to midcell. Pom1p also phosphorylate Cdr2p to promote Cdr2p-Mid1p interaction at midcell.

An anillin-like protein, Mid1p is the key player in ring positioning in *S. pombe*. During interphase, Mid1p actively shuttles in and out between the nucleus and adjacent cell cortex. In early mitosis, Mid1p is released from the nucleus and interacts with medial cortical nodes to recruit contractile ring components [71-73]. Mid1p acts as a spatial cue that integrates cell geometry and nuclear position to enable cell division at the appropriate cellular location. Microtubules determine nuclear positioning by exerting balanced pushing forces in the cylindrical fission yeast cells [74]. Cell centrifugation has been performed to document ring localization when nuclear position is displaced from middle of cells [71]. These experiments showed a shift in location of ring assembly according to nuclear displacement, suggesting that nuclear position

could be a determinant of the position of ring assembly [71, 75, 76].

Regulation of Mid1p results from coordination of various proteins such as Polo-like kinase Plo1p, SAD kinase Cdr2p and polarity protein kinase Pom1p. At interphase, Cdr2p binds to the plasma membrane as nodes with its C- terminus, forming a wide cortical band in the middle of the cell [77], while interaction of Cdr2p with Mid1p occurs through its N-terminal region [77, 78]. At the cell tip, Pom1p phosphorylates Cdr2p to reduce Cdr2p membrane affinity and down-regulate Cdr2p clustering ability, by modulating Cdr2p-Mid1p interactions [78]. Pom1p forms a concentration gradient down the long axis of the cell, which favours Mid1p accumulation away from the cell tips [79]. At mitotic entry, Plo1p triggers Mid1p exit from the nucleus [80]. This leads to Mid1p localization on the medial cortex surrounding the nucleus, where it recruits other contractile ring precursors. In early mitosis, these precursor nodes mature with addition of myosin II Myo2p, IQGAP Rng2p, F-BAR protein Cdc15p, and formin Cdc12p.

Another pathway contributing to the localization of division site is the tip occlusion pathway. This pathway involves cell-end-localized polarity factors Tea1p, Tea4p and Pom1p [81]. Pom1 mediates the phosphorylation of Cdc15p at the cell tip to enhance Cdc15p dynamics. This promotes Cdc15p localization to medial cortical nodes, where it mediates recruitment of formin Cdc12p, an actin-filament-nucleating protein [82]. At metaphase, nucleation of actin filaments causes the broad band of cytokinetic nodes to coalesce into a tight ring at middle of the cell [83].

Anchoring of the actomyosin ring involves the cooperation between Cdc15p with paxillin Pxl1 and β-glucan synthetase Bgs1p/Cps1p [84, 85]. It has been proposed that Cdc15p is required to transport Bgs1p from the Golgi apparatus to the plasma membrane [85].

The ring is unstable until all Bgs1p proteins are transported to the cell cortex [85]. Therefore the activity of Pxl1p coalescing myosin and actin bundles is facilitated by Cdc15p.

Collectively, fission yeast *S. pombe* is equipped with many pathways to ensure the fidelity of actomyosin ring localization. Division site placement is carried out under the guidance of spatial cues that relate cell geometry with nuclear position, as well as negative signaling pathways that prevent cell division at the cell tip.

1.4 FISSION YEAST CELL DIVISION

1.4.1 Actomyosin ring precursors

In fission yeast, there are two types of contractile ring precursors that determine the division plane positioning. Type I nodes consist of Cdr1p, Cdr2p and Mid1p. During interphase, type I locate in broad bands around the nucleus, at the medial region of the cell. Mid1p is exported from the nucleus to the cortical membrane to join the type I nodes. Cdr2p and Mid1p promote the recruitment of other ring assembly components, namely Wee1 kinase and its inhibitor, the Sad kinase Cdr1/Nim1, and type II nodes.

Type II nodes consist of Blt1p, Gef2p and Klp8p. Blt1p binding to membrane relies on a membrane binding domain located in C-terminus and its tetramerizing properties [72, 86-88]. These characteristics enable Blt1p to form nodes independently from Cdr2p [88]. During interephase, 75% of type II nodes superimpose with type I nodes at midcell, while the rest of the nodes are located at the new end [89].

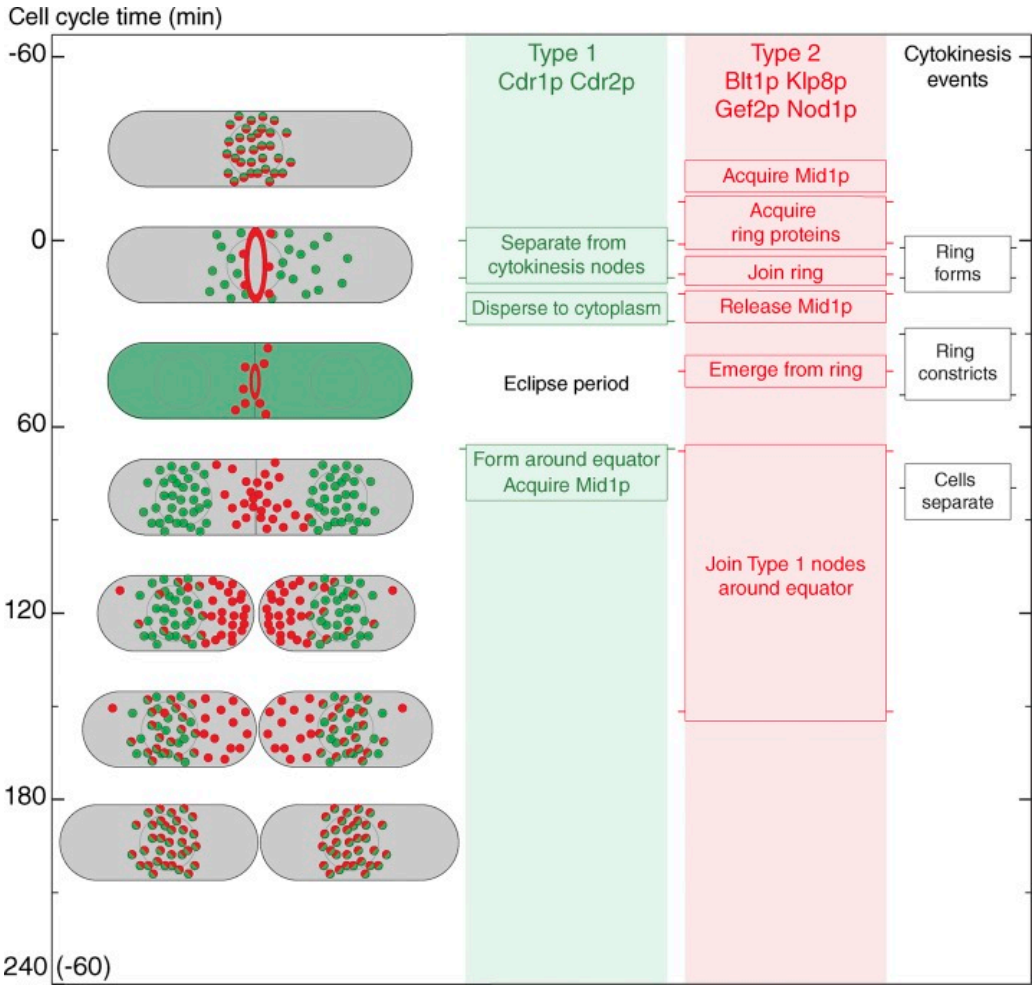

Figure 1.1 The contractile ring precursor nodes and their cell cycle oscillation.

Green dots represent Type 1 nodes while red dots represent type 2 nodes. Y-axis shows the timing of events. (Source: Illustration taken from Akamatsu et al., J Cell Biol., 2014)

1.4.2 Actomyosin ring formation

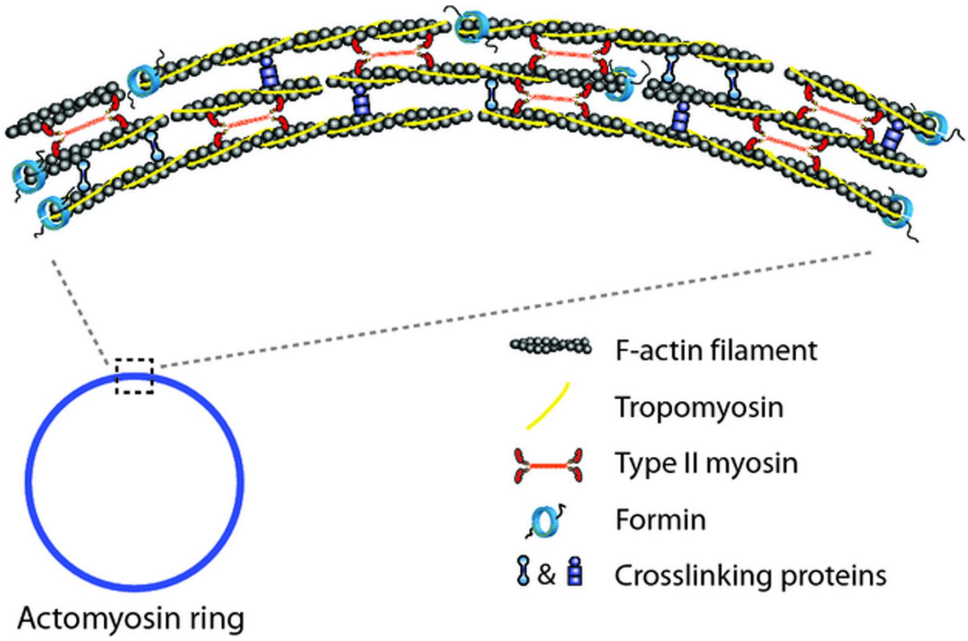

Figure 1.5 Components of an actomyosin ring.

In early mitosis actin filaments accumulate in the medial region of *S. pombe*. Formins nucleate these filaments from their barbed ends. Filaments are bundled by crosslinking proteins. Tropomyosin stabilizes actomyosin interaction. Motor protein myosin is involved in maintenance and constriction of the ring (Source: Illustration taken from Mishra, Huang and Balasubramanian, FEMS Microbiology Reviews, 2014).

The actomyosin ring is a cytoskeletal structure composed of more than 100 different proteins species. It is formed by condensation of the aforementioned nodes into cytokinesis nodes and later into a tight ring. When the node coalesce, actin filaments, motor protein myosin, actin-nucleating proteins, actin crosslinkers and other regulators of ring constriction join the broad band [90]. The actin-bundling protein IQGAP

Rng2p arrives and facilitates recruitment of type II myosin heavy chain (Myo2p) and regulatory right chain (Rlc1p).

Together with Rng2p, the F-BAR protein Cdc15p recruits the actin-nucleating protein Formin Cdc12p. Cdc12p is thought to participate in the Search-Capture-Pull-Release (SCPR) model of actomyosin ring formation [90]. Actin exists as patches and filaments in fission yeasts [91-95]. Actin filaments (F-actin) is a product of polymerization of actin monomer (G-actin). Each actin monomer has tight binding sites that facilitate interactions with two other actin monomers. Cortical actin patches accumulate at polarized growing cell tips [91], while actin filaments are nucleated from the cell tips and orientated parallel to the long-axis of the cell [91, 93, 96-98]. Actin filaments behave like elastic rods with a persistence length of 5-18 μm [99-102], and have been shown to favour localizing at the cortex when in a confined space [103]. It is proposed that Cdc12p nucleates actin filaments from nodes, and the growing actin filaments are captured by myosin molecules from neighbouring nodes. This connection allows the nodes to be compacted into actomyosin ring [90, 104].

Meanwhile, actin crosslinking proteins such as α-actinin-like protein (Ain1p) and fimbrin (Fim1p) mediate organization of actin filaments into bundles [105]. Tropomyosin (Cdc8p) binds to actin filaments and stabilizes actomyosin interaction (Stark et al., 2010). Myosin motors act on actin filaments to generate the driving force for actomyosin contraction.

1.4.3 Actomyosin ring maturation

The actomyosin ring does not contract immediately after tight ring formation. Actomyosin rings remain of the same diameter for 25 minutes

at maturation stage. The Cdc15p concentration in the ring increases about five fold while other proteins such as Myp2p, capping protein, septins and Arp2/3 complex are recruited to the ring or its close vicinity [1, 106]. Septation initiation network (SIN) triggers the ring contraction. It has been reported that SIN signaling is not required for nodes to coalesce into a compact ring structure, but the F-BAR protein Cdc15-p is accumulated less in the ring and ring contraction fails in SIN mutants [107-111]. SIN activity is important to stabilize fully formed actomyosin rings, as well as maintain the timely onset of actomyosin ring contraction [111].

1.4.4 Actomyosin ring contraction

SIN activity initiates ring contraction centripetally inwards, with force driven by myosin motors. Myo2p is the major motor for ring contraction [112-116]. Work done by Palani and colleagues demonstrated that the ring constrict with ATP-dependent motor activity of Myo2p. Mutation in Myo2p that compromised the ATPase activity resulted in failure of ring contraction *in vivo*, and does not support ATP-dependent actin filament motility *in vitro* [113].

Computational studies have been done to look at the actomyosin ring contraction mechanism. It was found that “actin-treadmilling” is involved in ring contraction, as this event further facilitates myosin to generate contractile forces by recruiting myosin clusters towards the pointed ends of actin filaments [117] .

1.4.5 Cell separation

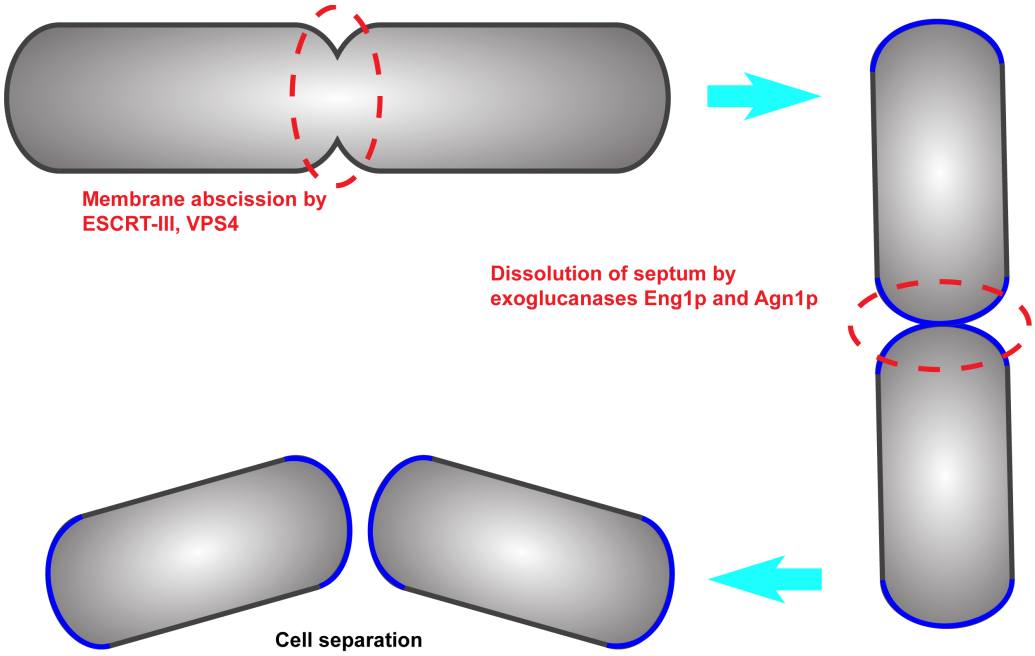

Figure 1.6 Cell separation facilitated by ESCRT abscission complex and exoglucanases.

ESCRT complexes - ESCRT-III and VPS4 drive membrane invagination at division site. Exoglucanases Eng1p and Agn1p degrade the septal cell wall material of daughter cells to enable complete cell separation.

Cell separation involves physical separation of plasma membrane as well as septum of daughter cells. In fission yeast, plasma membrane abscission is facilitated by endosomal sorting complexes required for transport (ESCRT complex) [118]. The ESCRT machinery consists of five multiprotein complexes that sequentially concentrate at membrane sites: ESCRT-0, ESCRT-I, ESCRT-II, ESCRT-III, and VPS4. The ESCRT-III complex has been demonstrated to comprise the core scission machinery and recruit VPS4. VPS4-dependent ESCRT-III

filament remodeling in turn drives membrane invagination and abscission[119-121].

Septum formation facilitates cell separation that comes after mitosis. It acts as the final tool to separate the daughter cells. In fission yeast, cell wall is made up of 1,3-β-glucan (50-54% of total polysaccharides) and 1,3-α-glucan (28-32%) [122-124]. The gene *cps1* encodes the catalytic subunit of β–glucan synthase, which is responsible for the synthesis of 1,3-β-glucan, a major component of the cell wall [125, 126]. Cps1p localizes at the actomyosin ring at midcell and is essential for primary septum formation. Its mutants are identified to be defective in cytokinesis. At permissive temperature, the *cps1*-191 mutants are unable to maintain constant cell diameter and a cylindrical morphology [125]. At non-permissive temperature, these mutant cells are arrested with two interphase nuclei as well as being more elongated than wild-type cells [127]. While the assembly of acytomyosin ring is unaffected, they are unable to form a division septum [125, 127].

The 1,3-α-glucan synthase in fission yeast is encoded by *mok1*. The *mok1* gene is also functionally closely related to Pck1 and Pck2, as it was identified during an attempt to screen for Pck1 and Pck2's downstream effectors [128]. The *mok1* mutant displayed abnormal cell shape and weak cell wall [128]. Therefore, both *cps1* and *mok1* are vital genes to maintain the integrity of cell wall and septum formation in fission yeast.

The final step in cell separation is the dissolution of primary septum and the erosion of cell wall materials surrounding the septum [129]. It is known that the 1,3-β-glucanase Eng1p is responsible for the dissolution of primary septum [130]. The Eng1p localizes to the medial region of the cell, around the septum, as well as the new ends of

daughter cells [131]. Cells lacking the *Eng1* function tend to clump [131]. The dissolution of cell wall surrounding the septum requires the 1,3-α-glucanase Agn1p [130, 132]. Clumping was also observed in the *agn1Δ* cells as a result of inefficient cell separation, as daughter cells remain attached via a small stretch of septum-edging material [130].

2. MATERIALS AND METHODS

2.1 YEAST STRAINS, MEDIA AND REAGENTS

2.1.1 Yeast strains

All *S. pombe* strains used in the study are listed in Table 2.1.

Genotype	Source	Strain number
ade6-210 ura4-D18 leu1-32 h-	Lab collection	MBY101
ade6-210 ura4-D18 leu1-32 h+	Lab collection	MBY102
clp1::ura4+ ura4-D18 leu1-32 ade6-21 h+	Lab collection	MBY977
rlc1::ura4 cyk3-GFP *h-*	Lab collection	MBY4763
mid1-GFP*:ura4+* mCherry-*atb2:hph*	Lab collection	MBY6462
Pact1-*lifeact*-EGFP*:leu1+* mCherry-*atb2:hph ura4-D18 leu1-32 h-*	Lab collection	MBY6659
Pact1-*lifeact*-EGFP*:leu1+* mCherry-*atb2:hph ura4-D18 leu1-32 h+*	Lab collection	MBY7114
mid1-18 Pact1-*lifeact*-EGFP*:leu1+* mCherry-*atb2:hph leu1-32*	Lab collection	MBY7161
cps1-191 *rlc1*-tdTomato-*natMX6* GFP-*psy1:leu1+ h+*	This study	MBY10138
cps1-191 *lifeact*-mCherry*:leu1+ h+*	This study	MBY10238
vps20::hph cps1-191 *rlc1*-tdTomato-*natMX6* GFP-*psy1:leu1+*	Lab collection	MBY10371
vps4::hph cps1-191 *rlc1*-tdTomato-*natMX6* GFP-*psy1:leu1+*	Lab collection	MBY10372
cps1-191 *rlc1::hph cyk3*-GFP	This study	MBY10383
eng1::kanMX4, *cps1*-191 *rlc1*-tdTomato-	Lab collection	MBY10417

natMX6 GFP-*psy1:leu1+*		
agn1::KanMX4, *cps1*-191 *rlc1*-tdTomato-*natMX6* GFP-*psy1:leu1+*	Lab collection	MBY10418
tea1-GFP:*KanMX6* mCherry-*atb2:hph h+*	This study	MBY11194
rlc1-GFP*:leu1+* mCherry-*atb2:hph h+*	This study	MBY11200
tea1::ura4+ Pact1-*lifeact*-EGFP*:leu1+* mCherry-*atb2:Hph h-*	This study	MBY11255
clp1::ura4+ Pact1-*lifeact*-EGFP*:leu1+* mCherry-*atb2:hph h-*	This study	MBY11627
tea1::ura4+ mid1-18 *pom1*-GFP*:KanMX6* mCherry-*atb2:hph h+*	This study	MBY11646
tea1::ura4+ mid1-18 *cdc3*-124 Pact1-*lifeact*-EGFP*:leu1+* mCherry-*atb2:hph h-*	This study	MBY11658
tea1::ura4+ mid1-18 *cdr2*-GFP*:ura4+* mCherry-*atb2:hph h-*	This study	MBY11666
cps1-191 *mok1*-664 *rlc1*-tdTomato-*natMX6* GFP-*psy1:leu1+ ura4-D18 ade6- h+*	This study	MBY12888
cps1-191 *hht*-GFP*:ura4+ rlc1*-tdTomato-*natMX6* GFP-*psy1:leu1+ ade6- h-*	This study	MBY12925

2.1.2 Culture media

S. pombe cells were grown in Yeast Extract with Supplements (YES). Selection of desired genotypes during tetrad dissection and random spore analysis were done on selection marker plates. Edinburgh Minimal Medium (EMMA) with required supplements, as well as YES containing antibiotics such as nourseothricin (nat), hygromycin B (hph) and kanamycin A (kan).

Cells were inoculated from YES media plates to liquid YES or selection medium two days before physiological experiment. The culture was then

diluted on the day before experiment. All liquid cultures were incubated in incubator shaker at 24˚C at 200RPM. Experiments were carried out when the OD_{595} of cell culture is 0.2 - 0.6 (roughly 4-12 x 10^6 cells/mL). For temperature shift experiments, cells were cultured to midlog phase before shifting to 36˚C.

All strains were stored in YES containing 15% glycerol and kept frozen in -80˚C.

2.1.3 Drugs and reagents

To severe actin filaments, Swinholide-A (Enzo Life Sciences, BML-T125-0020) was used at a final concentration of 10μM in all experiments. To slow down plasma membrane invagination, Brefeldin A (Fisher Scientific, 15526276) was diluted with culture media and used at 75μM in all experiments.

2.2 YEAST GENETICS METHODS

2.2.1 Genetic crosses

A new strain can be obtained by carrying out genetic crossing (Moreno et al, 1991). Mating was done by mixing two heterothallic strains of h+ and h-. Strains were scrapped from inoculation patches on YES plate and mixed evenly in 10μL sterile water. The mixture was then dropped on to ELN (Exocet Low Nitrogen) medium and incubated in 24°C for two to three days. All fluorescently-tagged strains generated were checked with microscope to confirm successful cross.

2.2.2 Tetrad analysis

Ascii was collected with a loop from the mating patch on ELN plate. Ascii was patched on a fresh YES plate in the form of a line. The plate was incubated in 36°C for 1 hour. For temperature sensitive mutants, the incubation at 36°C was not more than 1 hour and 10 minutes. Tetrad dissection was subsequently carried out with a Singer Micromanipulator (MSM 400, Singer instrument). YES plates were then kept in 24°C for 6-8 days to allow colony germination. Target genotype was then selected by replicating the colonies to different selection marker plates and conditions.

2.2.3 Random spore analysis

To obtain a strain by random spore, a large portion of the mating patch was collected from ELN and mixed in 1mL of sterile water. 10µL of Glusulase (Perkin Elmer, NEE154001EA) was added to the tube, the tube was then kept in room temperature on a rotator at 14RPM. After 11 hours, spores were washed with 40% ethanol to remove possible contaminants, subsequently washed twice with sterile water. Spores were resuspended in 1mL sterile water. 1µL of spore is mixed with 249µL sterile water to make a 1:250 dilution. 10µL of spore was spreaded on YES plates. The plates were then kept in 24˚C for 6-8 days to allow colony germination. Target colony was then selected by replicating the colonies to different selection marker plates and conditions.

2.3 YEAST CELL BIOLOGY METHODS

2.3.1 *S. pombe* spheroplast preparation

S. pombe cells were grown at 24˚C to mid-log phase, with OD_{595} 0.2 – 0.4. 20mL of cells were collected at 3000rpm for 1 minute. Cells were washed with equal volume of 1X E-Buffer (50 mM sodium citrate and 100 mM sodium phosphate, pH 6.0) and 1X E-Buffer containing 0.6M sorbitol, before

resuspending in 5mL of 1X E-Buffer supplemented with 1.2M sorbitol. 30mg of lysing enzyme (Sigma, L1412) was weighed and added into the culture. Cells were incubated at 24˚C (or non-permissive temperature for temperature sensitive mutants), shaking at 80RPM. After 1.5 hour, 30µL of LongLife Zymolyase (GBiosciences, 1.5 U/µL) was added, and cells were incubated for another 1.5 hour. The following washes were done with centrifugation at 450xg for 2 minutes each time. Protoplasts were washed with 1X E-buffer with 0.8M sorbitol, then resuspended in 10mL EMMA supplemented with 0.8M sorbitol. 0.5% 2-deoxy-D-glucose (2DG) (Sigma, D6134) was subsequently added to the culture. Spheroplasts (when protoplasts generated are spherical) were incubated for 30 minutes before proceeding to slide preparation and image acquisition.

2.3.2 Spheroplast fixation of *S. pombe* for electron microscopy

250mL of cells with OD_{595} 0.2 were collected for spheroplasting. Spheroplasts were prepared with the protoplasting method described above. Spheroplasts were spun down from EMMA with 0.8M sorbitol and resuspended in phosphate-buffered saline (PBS) with 2.5% glutaraldehyde and 1.2M sorbitol. After 2 hours incubation at room temperature, spheroplasts were spun down in round bottom tubes. The following procedure were done on ice and gently (vortex mixer is avoided). Spheroplasts were resuspended in fix solution (PBS containing 2% glutaldehyde and 1.2M sorbitol) and stood on ice for 2 hours. The spheroplasts were separated into 2 tubes: washed and unwashed samples. Unwashed samples were stored at 4°C. The washed samples were washed with 1mL PBS containing 1.2M sorbitol for three times. Lastly the spheroplasts were resuspended in 1mL PBS containing 1.2M sorbitol and stored at 4°C before EM.

2.3.3 Cell fixation of *S. pombe*

Cells were cultured to a density of 0.2~0.4 at OD_{595} and spun down at 3400rpm for 3 minutes. After washing the cells with PBS of equal volume, 500μL of PBS and 500μL of 8% PFA (paraformaldehyde) were added to the cells. Cells were fixed in PFA for 12 minutes at room temperature. To remove excess PFA, the cells were washed with PBS for 3 times and resuspended in 100μL PBS. Fixed cells were stored at 4˚C.

2.3.4 Cell permeabilization of *S. pombe*

To 100μL of cells in PBS, 100uL of 1% Triton X-100 (Sigma, diluted in 1x PBS) was added, so that cells to solution ratio is 1:1. Cells were incubated on ice for 10 minutes, then spun down at 3400 rpm for 3 minutes to remove Triton X-100. Cells were washed with PBS for 3 times and resuspended in 15 - 25μL PBS.

2.3.5 Staining *S. pombe*

After fixation, the cells were added with 4', 6-diamidino-2-phenylindole (DAPI) at 1μg/mL. Actin structures were stained by adding CF633 (Biotium, #00046) to the fixed cells. Cell wall is stained with 1% (w/v) calcofluor white (Sigma Aldrich, #18909) by adding it at 100x dilution into 10μL of cells in PBS.

2.4 MICROSCOPY DATA ACQUISITION AND ANALYSIS

2.4.1 Time-lapse movie cell suspension preparation

Cells were collected and concentrated by centrifugation at 3,000RPM for 1 minute. Spheroplasts were collected and concentrated by centrifugation at 450xg for 2 minutes. 12μL of cells or spheroplasts were loaded onto an Ibidi

μ-Slide 8-Well glass botton dish (Cat. No. 80827). To prevent evaporation, the sample was covered with 400μL mineral oil (Sigma, M5310) prior to imaging.

2.4.2 Time-lapse movie slide preparation

Slide was prepared by placing YES with 2% agarose pad on a concave glass slide (Academy Microscope Slides, N/A 144). Cells were collected and concentrated by centrifugation at 3,000RPM for 1 minute. Spheroplasts were collected and concentrated by centrifugation at 450xg for 2 minutes. 1.2μL of cells or spheroplasts were dropped onto the medium and sealed with a coverslip using VALAP (equal mixture of Vaseline, lanolin and paraffin) prior to imaging.

2.4.3 Spinning dick confocal microscopy

The spinning disk confocal system was equipped with the Nikon ECLIPSE Ti inverted microscope, Nikon Plan Apo λ 100x /1.45 NA oil immersion objective lens, a spinning-disk system (CSU-XZ1; Yokogawa) and an Andor iXon Ultra EMCCD camera. Images were acquired using the Andor iQ3 Live Cell Imaging software at the pixel size of 69nm/pixel or 80nm/pixel. To illuminate fluorophores, laser lines at wavelengths of 488nm (GFP, green fluorescent proteins), 561nm (RFP, red fluorescent proteins) and 633nm (far-red fluorescent proteins) were used for excitation. Images were acquired with a Z-range of 7 - 10μm with a step size of 0.3 – 0.5μm.

2.4.4 Total internal reflection fluorescence (TIRF) microscopy

The Andor Revolution TIRF system was equipped with the inverted Nikon Eclipse microscope base, Nikon Apo 100x /1.49 NA Apo TIRF objective lens, a motorized single line Nikon TIRF module, a 60mW 488nm solid state Laser and an Andor Zyla sCMOS camera. Images were acquired using Andor

iQ3 software at the pixel size of 65nm/pixel. The TIRF microscopy was done at room temperature.

2.4.5 General image processing and data analysis

Images were viewed and analyzed using ImageJ (https://imagej.nih.gov/ij/). All time-lapse movies were maximum projected with Andor iQ3 Life Cell Imaging Software. If applicable, the movies were bleach corrected using "Plugins/Stacks-T-Functions/Bleach Correction" plugin in imageJ. To measure ring circumference, a straight line is drawn across the ring to obtain diameter. All still images and time-lapse movies were edited by ImageJ. Graphs were plotted using GraphPad Prism 6 (https://www.graphpad.com/scientific-software/prism/).

3. EQUATORIAL ASSEMBLY OF THE CELL-DIVISION ACTOMYOSIN RING IN THE ABSENCE OF CYTOKINETIC SPATIAL CUES

3.1 INTRODUCTION

In fission yeast, the actomyosin ring is always positioned at the cell middle to enable medial division, and assembly of this ring is aided by spatial cues, such as from Mid1p and the tip complex [71, 73, 81, 133, 134]. At mitotic entry, Mid1p binds to the cell membrane adjacent to the nucleus and associates with ring precursors also known as medial cortical nodes [71, 72, 80, 135]. These ring precursors are restricted to the medial region of the cell by the tip complex [81]. Mid1p is the key player acting as the positive cue for actomyosin ring assembly, by associating cell geometry and nuclear position with the recruitment of ring components [71].

Additionally, the tip complex, comprised of Tea1p, Tea4p and Pom1p, acts as a negative cue at the cell tips, by reducing the likelihood of Mid1p localizing to these areas, thereby promoting recruitment of ring components to the medial cell cortex [81]. The essential ring component Cdc15p is hyperphosphorylated in interphase, then hypophosphorylated before actomyosin ring formation for medial localization [136, 137]. Studies have been performed to observe septum assembly in cells lacking either Mid1p or tip complex functions, however, the effect of losing both spatial cues simultaneously on the localisation of actomyosin ring is yet to be investigated [73]. It is the factors responsible for guiding the location of ring assembly when the known spatial cues are absent that we are interested in investigating.[91]

Because actomyosin ring positioning, ring assembly, and cell morphogenesis are genetically separable in fission yeast, we were able to derive actomyosin ring placement mechanisms from first principles. In this report, we showed that during ring assembly in the absence of cytokinetic cues (anillin-related protein Mid1 and tip-complex proteins), actin bundles follow the path of least curvature and assemble actomyosin rings in an equatorial position in spherical protoplasts and along the long axis in cylindrical cells and compressed protoplasts. The equatorial position of rings is abolished upon treatment of protoplasts with an actin-severing compound or by slowing down actin polymerization. We propose that the physical properties of actin filaments/bundles play key roles in actomyosin ring assembly and positioning and that key cytokinetic molecules may modulate the length of actin filaments to promote ring assembly along the short axis.

3.2 RESULTS

3.2.1 Actomyosin rings were assembled equatorially in wild-type spheroplasts.

In *S. pombe*, cell geometry, cell wall and cytokinesis-positioning factors mediate the localization of the actomyosin ring [138-142]. To investigate the impact of removing the known localization factors on contractile actomyosin rings, we attempted to perturb the cell morphology by changing it from cylindrical to spherical. To achieve this, fission yeast spheroplasts were prepared by enzymatic digestion of the yeast cell wall glucan. In yeasts the cell wall is solely responsible for determining the cell shape, and in its absence (or near absence) the cells become spherical in order to minimise the average curvature, and therefore the elastic bending energy, of the cell membrane.

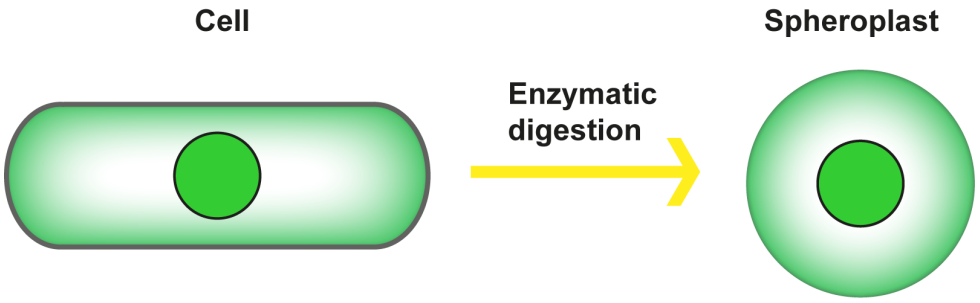

Figure 3.1 Yeast spheroplast transformation.

Cells were treated with lysing enzyme to hydrolyze the cell wall β-glucan. Rod-shaped cells became spherical.

As in higher eukaryotes, the contractile actomyosin ring is formed by the nucleation of F-actin filaments at the division site, and the shaping of these filaments into a tight ring, along with myosin II [44]. Therefore, we opted to visualize the ring with wild-type cells expressing

either *lifeact*-GFP, as a marker of actin structures, or *rlc1*-GFP as a marker of the myosin regulatory light chain, whilst mCherry-Atb2 (alpha-tubulin) was also used as a marker of the cell-cycle stage. The *lifeact*-EGFP (Figure 3.2) and *rlc1*-GFP tagging did not cause any detectable cytokinetic defects in cells, and we therefore decided to use these for our experiments, where time-lapse microscopy was performed to observe ring assembly in spheroplasts generated from wild-type cells.

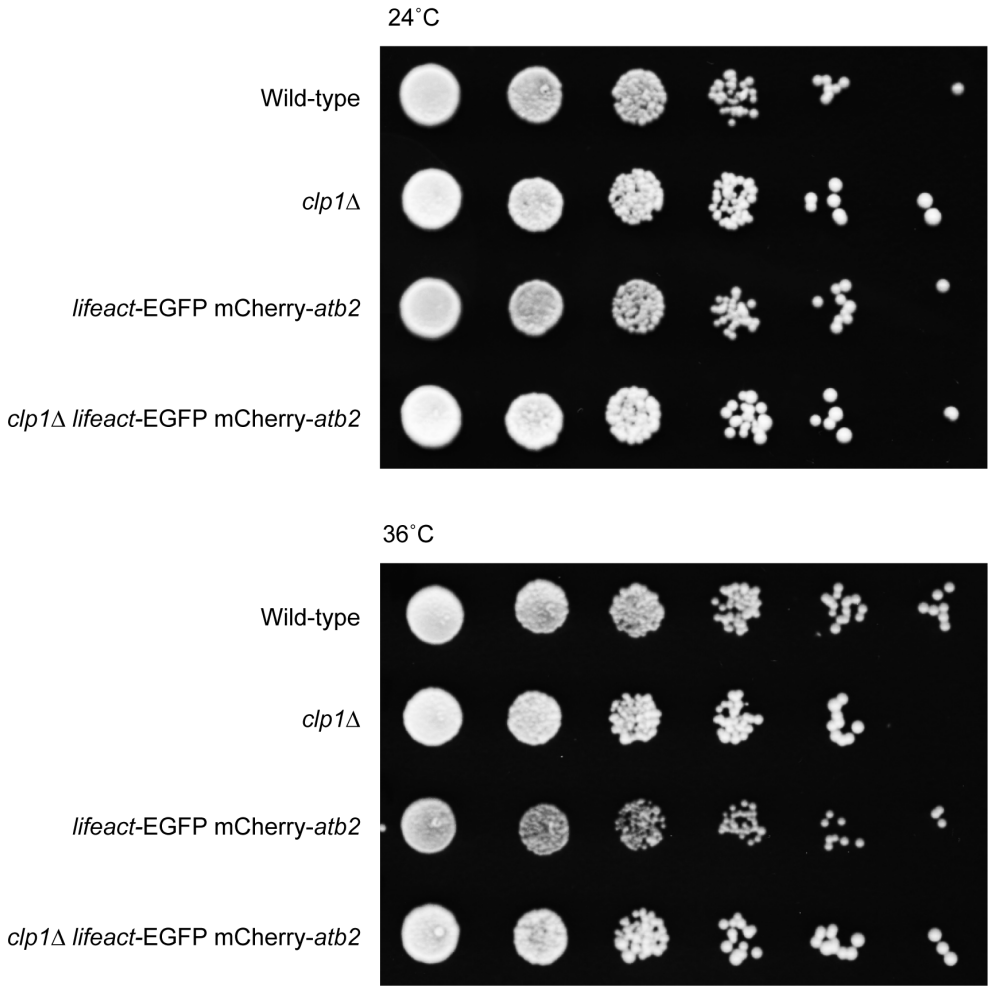

Figure 3.2 Analyses of the effects of the *lifeact*-EGFP expression in cells.

Wild-type, *clp1Δ*, *lifeact*-EGFP mCherry-*atb2*, and *clp1Δ lifeact*-EGFP mCherry-*atb2* cells were serially diluted, spotted on two YE agar plates, and incubated at 24°C and 36°C respectively. The *lifeact*-EGFP driven under the *S. pombe* actin promoter was used to label actin filaments. To test if expression of *lifeact*-EGFP under the actin promoter caused any cytokinetic defects, *lifeact*-EGFP was expressed in cells lacking Clp1 phosphatase. The *clp1*-null cells were previously shown to be sensitized to mild cytokinetic perturbation. There were no noticeable cytokinetic defects observed in *clp1*-null cells expressing *lifeact*-EGFP.

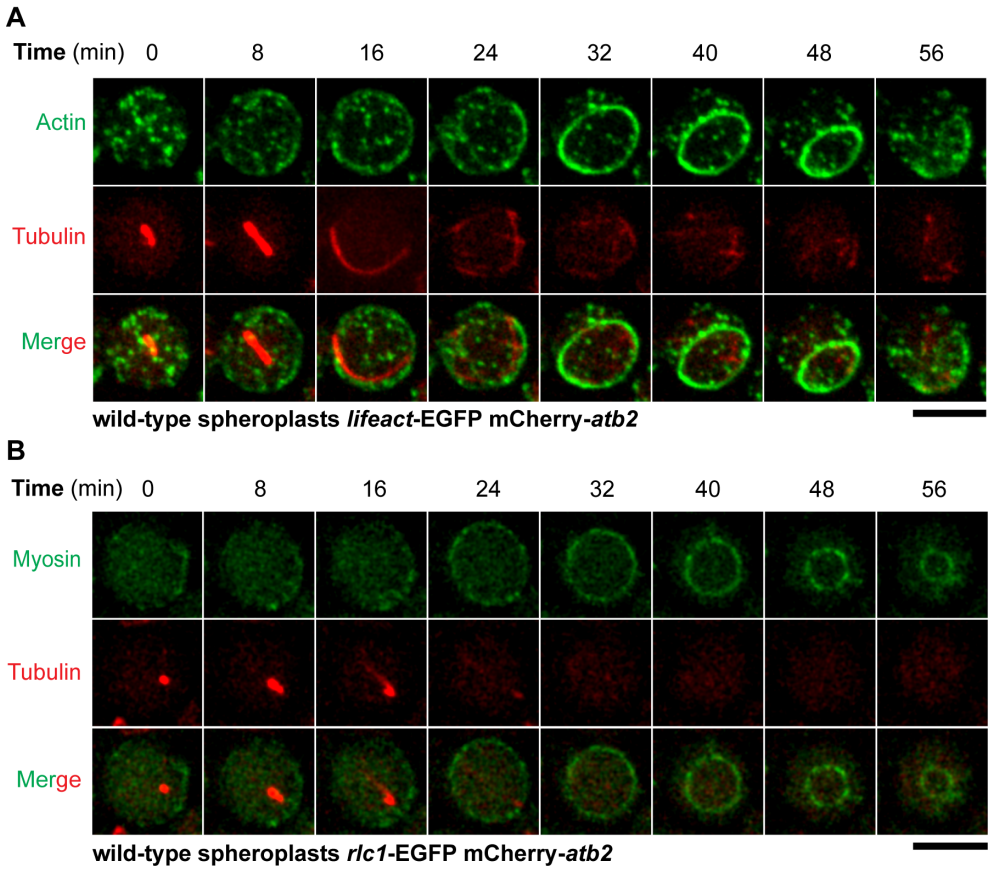

Figure 3.3 Time-lapse microscopic images of representative spheroplasts.

(A) A wild-type spheroplast expressing *lifeact*-EGFP (actin) and mCherry-Atb2 (tubulin) imaged at 36˚C (quantification is shown in Figure 3.4, n = 116). Time 0 minute indicates spheroplast enter anaphase stage, where spindle elongates.

(B) A wild-type spheroplast expressing Rlc1-EGFP (myosin) and mCherry-Atb2 (tubulin) imaged at 36˚C (quantification is shown in Figrue 3.4, n = 60). Time 0 minute indicates spheroplast enter anaphase stage, where spindle elongates.

Scale bars = 5 μm.

To compare the ring size with spheroplast size, ring and spheroplast diameters were measured to obtain circumferences. Ring

diameters (R) were visualized and measured by either *lifeact*-EGFP or Rlc1-EGFP. The diameter of spheroplast (S) is defined as the length of a line through the centre of the spheroplast that intersects two points on its circumference. This was acquired by measuring the perpendicular axis across R. The ratio of these parameters (R/S) was used to demonstrate the size of the ring in comparison to the diameter of the spheroplast (Figure 3.4). An R/S of 0.85 was selected as the cut-off for equatorial assembly of the ring. As spheroplasts progressed through mitosis, as indicated by the appearance and elongation of the mitotic spindle, the actin ring assembled at an equatorial position very close to the path of maximum circumference in 90% of the spheroplasts. *lifeact*-EGFP and Rlc1-EGFP showed average R/S values of ~0.93 ± 0.08 and ~0.93 ± 0.09 respectively (Figure 3.4). The rings slid across the membrane as they contracted, and subsequently disassembled, consistent with previous work [139].

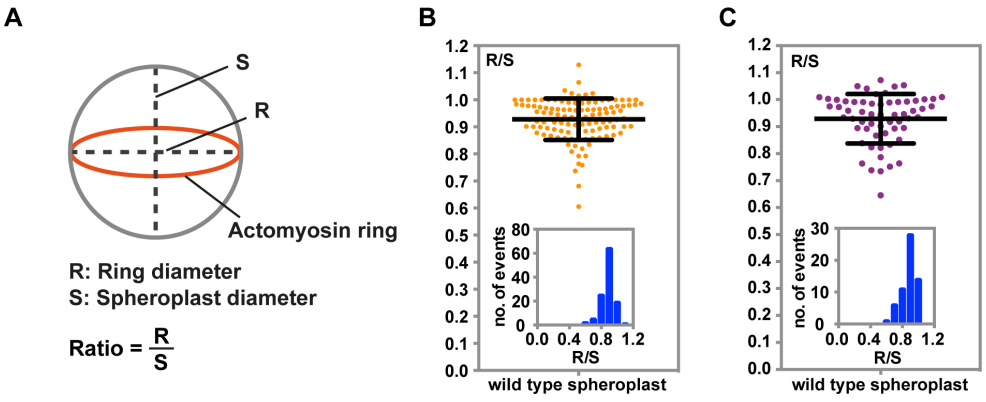

Figure 3.4 Quantification of R/S ratios of spheroplasts.

(A) Sketch of diameters of the rings (Rs) and spheroplasts (Ss). R and S are measured and compared. The ratio of R/S is used to indicate the size of the newly assembled rings. When the ratio is close to 1, it indicates the equatorial positioning of a ring.
(B) The R/S ratio of spheroplasts expressing *lifeact*-EGFP (actin) and mCherry-Atb2 (tubulin) (n = 116).

(C) The R/S ratio of spheroplasts expressing *rlc1*-GFP (myosin) and mCherry-Atb2 (tubulin) (n = 60).

Error bars indicate SD.

3.2.2 Mid1p and Tea1p are mislocalized in spheroplasts.

For the visualization of Mid1p and Tea1p in cells and spheroplasts, we utilized yeast strains expressing GFP fluorescence markers attached to these proteins. In an intact cell, Mid1p was readily detected as a broad band at the medial region of the cell during early mitosis, which subsequently coalesces into a compact ring during late mitosis (Figure 3.5). To confirm the specific localization of Mid1p, a line superimposing the cell periphery was drawn to generate fluorescence intensity plots. Two distinct peaks were detected, indicating the controlled localization of Mid1p at a fixed area in the cell. A similar phenomenon was observed in the intensity plots of Tea1p, where Tea1p was shown to be concentrated at cell ends. However, such organized localization was not observed in spheroplasts, where Mid1p and Tea1p seemed to be distributed randomly across the cell membrane. Fluorescence intensities plots of Mid1-GFP and Tea1-GFP confirmed the proteins' mislocalization in spheroplasts.

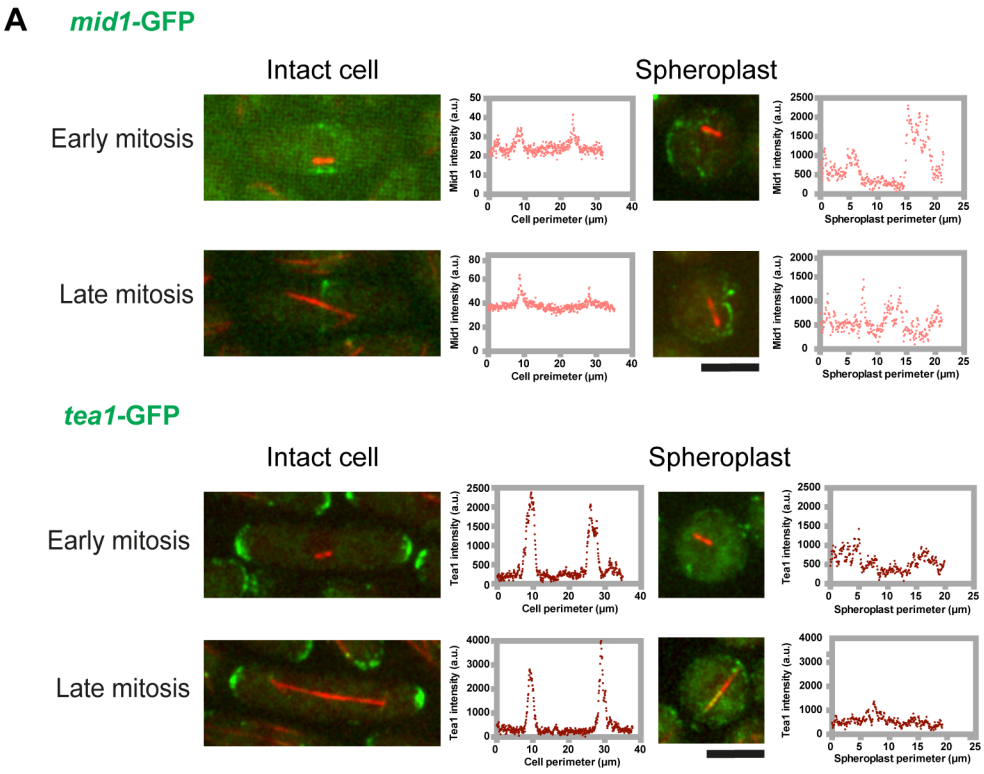

Figure 3.5 Localization of Mid1p and Tea1p.

In an intact cell, Mid1p and Tea1p localize at the actomyosin ring and cell tips respectively. The plots next to fluorescence images shows the distribution of Mid1p and Tea1p fluorescence signals along cell periphery.

Scale bars = 5 μm.

3.2.3 Equatorial assembly of contractile actomyosin rings in spheroplasts defective in *mid1* and *tea1* functions.

Although Mid1p and Tea1p appeared to be mislocalized in wild type spheroplasts, it was possible that trace amounts of these proteins could still promote the equatorial assembly of contractile actomyosin rings. To test this hypothesis, we studied ring assembly in *mid1*-18 (a temperature-sensitive allele) mutant spheroplasts that were defective in the functions of Mid1p. Interestingly, time-lapse microscopy revealed

that the majority of *mid1*-18 spheroplasts were able to assemble a ring (Figure 3.6, panel A), and about 90% of rings were assembled with R/S ~0.93 ± 0.06 (Figure 3.6, panel A). We then proceeded to investigate the role of *tea1* in ring assembly by imaging *tea1*-null mutants. We found that its absence did not cause an apparent phenotype on ring assembly (R/S ~0.89 ± 0.12) (Figure 3.6, panel B). Previous studies detected a synthetic lethal interaction when both *mid1* and *tea1* are deleted (Huang et al., 2007). Therefore, to further investigate ring assembly in spheroplasts lacking Mid1p and Tea1p, we constructed a double mutant of *mid1*-18 and *tea1Δ.* Phenotypes were profiled using time-lapse microscopy of spheroplasts expressing LifeAct-GFP and Rlc1-tdTomato (Figure 3.6, panel C). Surprisingly, ~84% of the spheroplasts assembled actomyosin rings with R/S ~0.91 ± 0.08 (Figure 3.6, panel C). Additionally, the F-BAR protein Cdc15 was also detected in conjunction with *rlc1*-GFP in the ring (Figure 3.6, panel D). These results established that both Mid1p and Tea1p are not essential in equatorial ring assembly in spheroplasts.

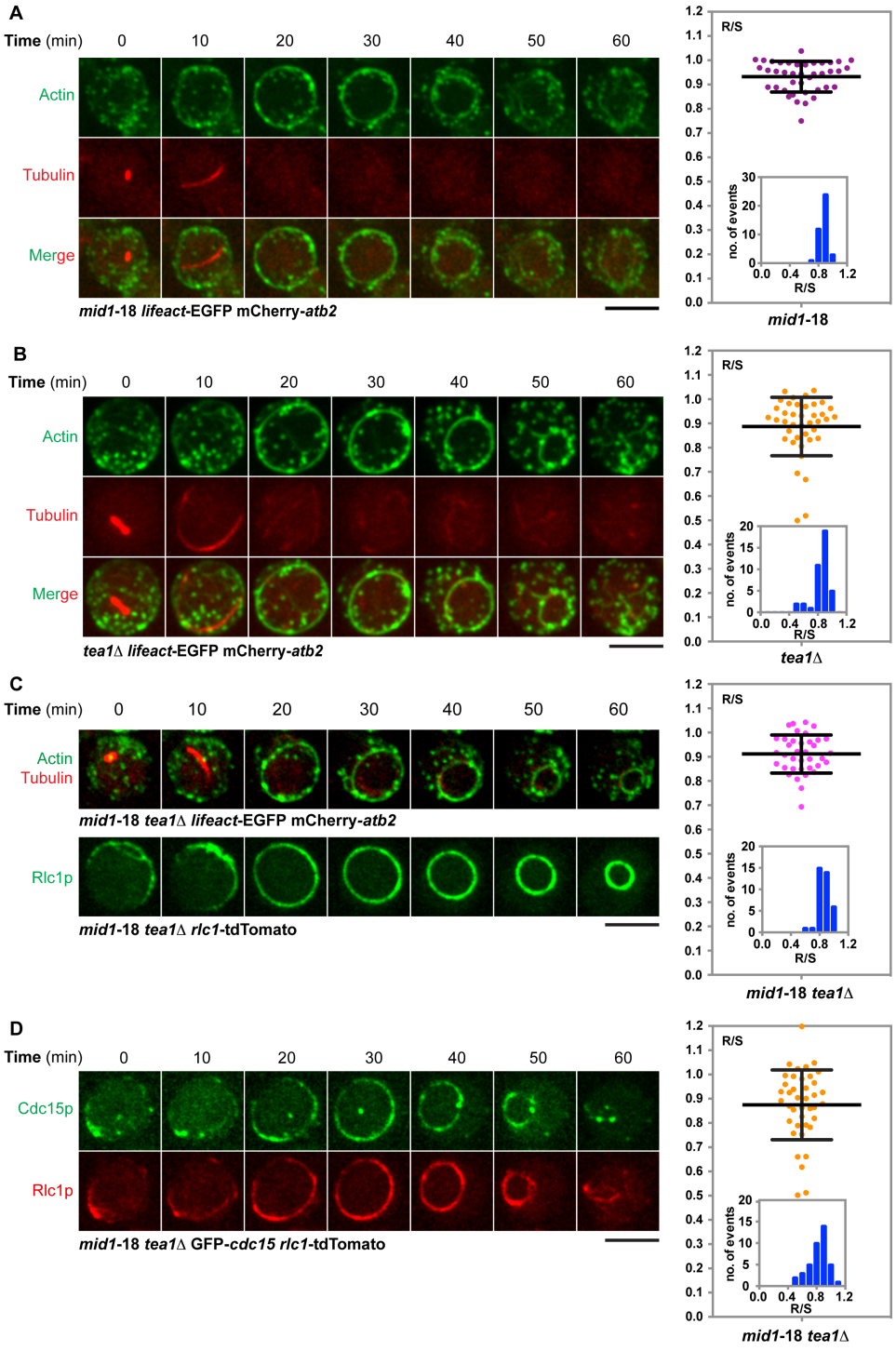

Figure 3.6 Equatorial Assembly of Actomyosin Rings in Spheroplasts Defective in Mid1p and Tea1p Functions.

(A) Time-lapse microscopic images of *mid1*-18 mutant spheroplasts expressing *lifeact*-EGFP (actin) and mCherry-Atb2 (tubulin) at 36˚C. The R/S ratio of spheroplasts is quantitated and plotted (n = 40).
(B) Time-lapse microscopic images of *tea1*-deletion mutant spheroplasts expressing *lifeact*-EGFP (actin) and mCherry-Atb2 (tubulin) at 36˚C. The R/S ratio of spheroplasts is quantitated and plotted (n = 40).
(C) Dynamics of F-actin (top) and Rlc1 (bottom) in *mid1*-18 *tea1Δ* spheroplasts at 36˚C. The R/S ratio of spheroplasts is quantitated and plotted (n = 37).
(D) Localization of Cdc15 (top) and Rlc1 (bottom) in *mid1*-18 *tea1Δ* spheroplasts at 36˚C. The R/S ratio of spheroplasts is quantitated and plotted (n = 44).

Scale bars = 5 μm. Error bars indicate SD.

3.2.4 SAD-kinase Cdr2 and DYRK family kinase Pom1 do not affect equatorial ring assembly in spheroplasts.

Given the assembly of actomyosin rings in spheroplasts with mislocalized Mid1p and Tea1p, we investigated the localization of the upstream regulators SAD-kinase Cdr2 and DYRK family kinase Pom1 in spheroplasts. The Cdr2 kinase and Pom1 kinase were distributed throughout the plasma membrane or were undetectable at non-permissive temperature (Figure 3.7). Thus, equatorial assembly of contractile actomyosin rings in spheroplasts is independent of Mid1p, Cdr2p, Pom1p and Tea1p functions.

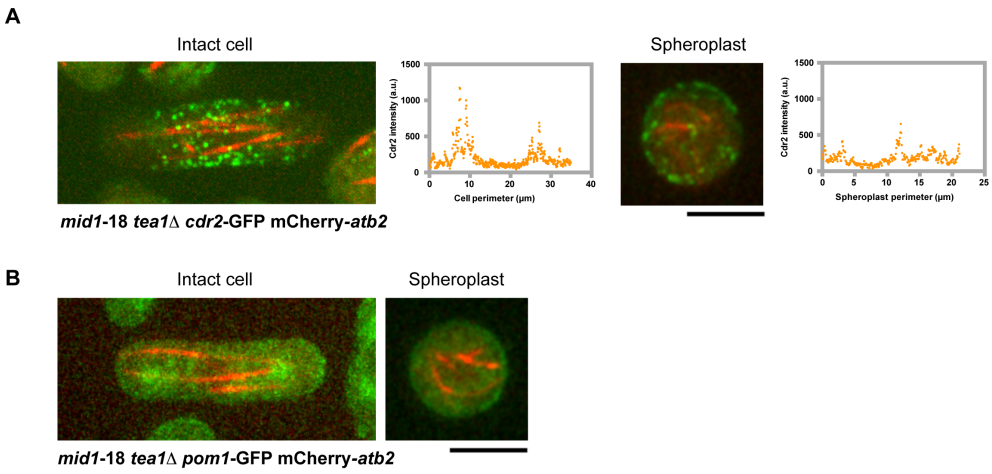

Figure 3.7 Localization of Cdr2 kinase and Pom1 kinase.

(A) Localization of Cdr2-GFP in *mid1*-18 *tea1Δ* intact cells and spheroplasts. Fluorescence intensities of Cdr2-GFP were measured along the cell perimeter. The image at the focal plane was selected for the intensity measurement.
(B) Localization of Pom1-GFP in *mid1*-18 *tea1Δ* intact cells and spheroplasts.

Scale bars = 5 μm.

3.2.5 Cdc15-Cdc12 interaction does not affect equatorial ring assembly in spheroplasts.

The F-BAR protein Cdc15p is known to bind membranes through its N-terminal F-BAR domain, and interacts with other proteins through its C-terminal protein-binding domains [143]. Localization of Cdc15p at the cell medial region influences the recruitment of formin Cdc12p to the division site [82], as mutation of a conserved proline within Cdc12p (P31A) was found to disrupt its interaction with Cdc15p *in vitro* [143]. Cells without the Cdc12-Cdc15 interaction showed delayed actomyosin ring formation [143].

We wondered whether ring assembly in spheroplast is further perturbed in cells lacking both Mid1p and Tea1p function, and the Cdc12-Cdc15 interaction. We therefore constructed a *mid1*-18 *tea1Δ Cdc12*-P31A mutant. Time-lapse microscopy at 36˚C showed ring assembly in spheroplasts of this mutant. Quantification of spheroplasts with ring formation revealed the importance of the Cdc12-Cdc15 interaction in the absence of *mid1* and *tea1* function. Among 56 spheroplasts observed, 45.6% of spheroplasts failed to assemble an actomyosin ring, 53.4% of spheroplasts assembled a ring. Among the spheroplasts that assembled a ring, 46.6% of them showed a ring to cell circumference ratio of ≥0.5, with an average ring to spheroplast circumference ratio of ~0.8 ± 0.2 overall (Figure 3.8).

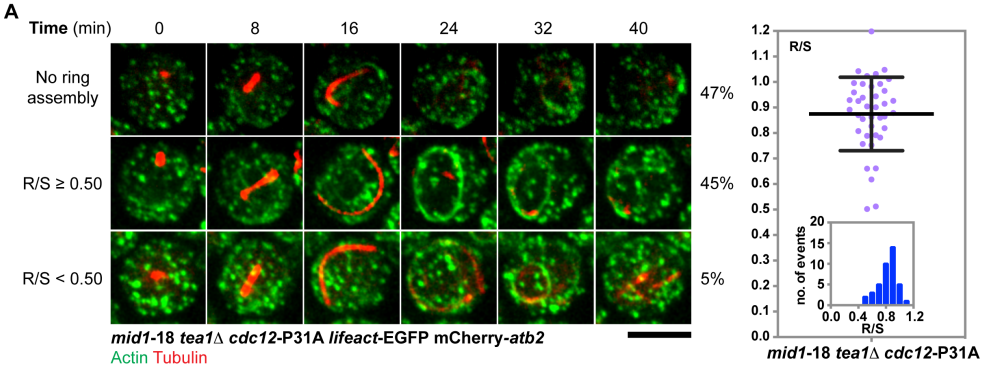

Figure 3.8 Actomyosin ring assembly in mutants lacking Cdc12p-Cdc15p interaction.

(A) Time-lapse imaging of *mid1*-18 *tea1Δ cdc12*-P31A cells expressing LifeAct-GFP and mCherry-*atb2* at 36˚C. Graph (right) reveals average ratio of ring to spheroplast circumference.

Scale bars = 5 μm.

3.2.6 There is no relationships between the spindle axis and ring assembly plane in spheroplasts.

It remained possible that the axes of anaphase spindles could influence location of ring assembly. We therefore quantified the timing of ring assembly in single mutants of *mid1*-18 and *tea1Δ* spheroplasts and *mid1*-18 *tea1Δ* double mutants, and found that all strains assembled rings at late mitosis, which is approximately 25-30 minutes after mitotic entry, as indicated by the formation of short mitotic spindles (Figure 3.9, panel A). However, we observed a wide range of inclination angles between the spindle axis and ring assembly plane, ranging from being parallel to being perpendicular to each other (Figure 3.9, panel B).

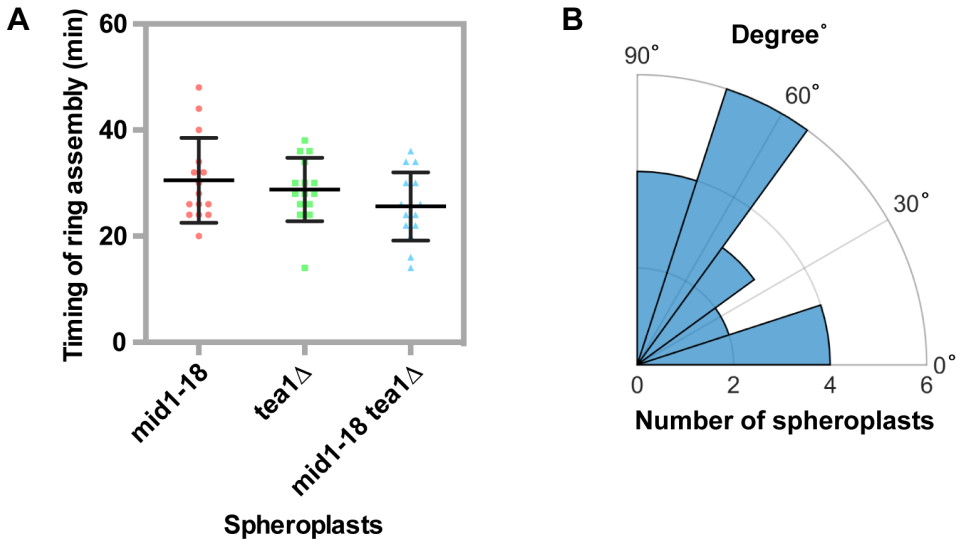

Figure 3.9 Quantification of Ring assembly timing and their inclination angles.

(A) Timing of ring assembly in *mid1*-18, *tea1Δ*, and *mid1*-18 *tea1Δ* spheroplasts.
(B) The inclination angles between the long axes of anaphase spindles and the plane of actomyosin rings in *mid1*-18 *tea1Δ* spheroplasts were measured and plotted (n = 20 spheroplasts).

Error bars indicate SD.

3.2.7 Severing actin filaments with swinholide-A.

Given the two major actomyosin ring-positioning mechanisms were not involved in equatorial positioning of the contractile actomyosin ring in spheroplasts, we sought to determine the mechanism that positioned the actomyosin ring at the equator in spheroplasts. Recent work by Ishiwata and colleagues provided insights into ring formation in spherical cells. They showed that F-actin-containing rings always assembled at the equator of cell-sized water-in-oil droplets. They proposed that actin filaments behave like a flexible polymer, assemble

along the path of least curvature to minimize the elastic bending energy of actin filaments. When the droplet is compressed, the actin rings assemble in the plane perpendicular to the compression, where the curvature of the droplet boundary is minimal.

We considered whether a similar mechanism may be working in fission yeast spheroplasts. If this were the case, severing actin filaments should result in non-equatorial assembly of actomyosin rings, as shorter actin filaments may be capable of forming rings with higher curvature. To further validate the hypothesis, we used actin-targeting drugs to perturb actin dynamics, and therefore alter the mechanical properties of actin filaments *in vivo*. Initially, we wished to create shorter actin filaments, through addition of the actin filament severing drug swinholide-A. Swinholide A has been reported to rapidly sequester actin dimers *in vitro* and disrupt the actin cytoskeleton (Bubb et al., 1995; Klenchin et al., 2005). We have recently developed a method to purify polymerization-competent *S. pombe* actin and human β-actin, so we decided to use these actins to characterize the effects of swinholide-A. We were able to observe actin filaments when purified G-actin was mixed with DMSO, $MgCl_2$, and ATP, however such polymers were not observed when G-actin was mixed with swinholide-A, $MgCl_2$, and ATP (Figure 3.10, panel A) (Experiment carried out by member of our group, Tomoyuki Hatano). These observations suggested that swinholide-A was either blocking actin polymerization or causing severing of fission yeast and human actin. To check whether swinholide-A severs actin filaments, we treated pre-assembled human actin filaments with swinholide-A. We observed severing of actin filaments when filaments in a flow chamber were treated with swinholide-A, while treatment with DMSO did not lead to the same observation (Figure 3.10, panel A).

These results established that swinholide-A caused actin filament severing.

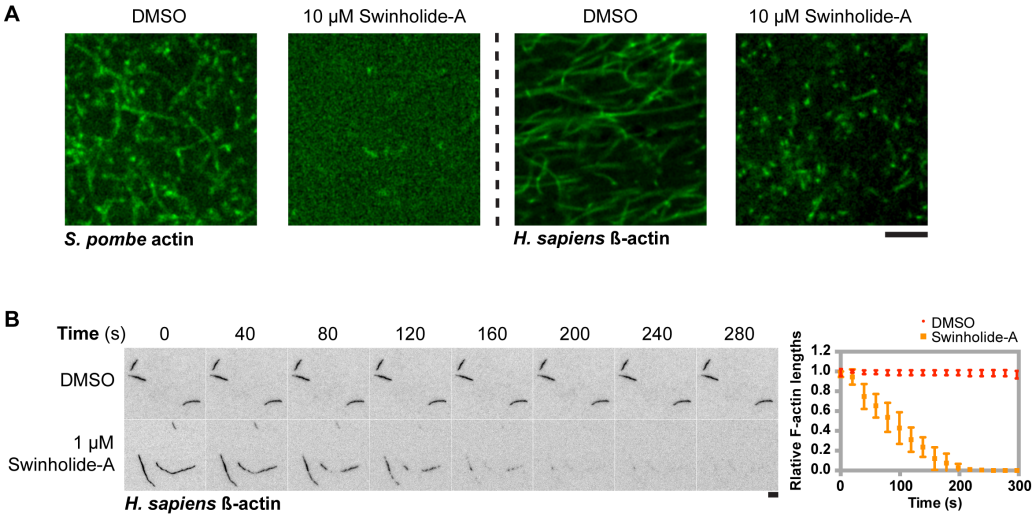

Figure 3.10 *In-vitro* Swinholide-A treatment of actin filaments.

(A) Purified *S. pombe* globular actin and *H. sapiens* beta-globular actin were incubated with DMSO or with 10 µM swinholide-A in the actin polymerization buffer and imaged by fluorescence microscopy.

(B) Pre-assembled actin filaments were treated with DMSO or with 1 µM swinholide-A, and imaged by total internal reflection fluorescence (TIRF) microscopy. The lengths of actin filaments after treatments were measured and normalized to their initial lengths, and their relative values were plotted as a function of time (n = 6 actin bundles/filaments for each treatment). (Figure provided by Tomoyuki Hatano)

Scale bar = 5 µm. Error bars indicate SD.

3.2.8 Swinholide-A treatment disrupts equatorial assembly of contractile actomyosin rings in spheroplasts.

Next, we investigated the effect of swinholide-A in *mid1*-18 *tea1Δ* spheroplasts. We assessed the position of contractile actomyosin rings

after swinholide-A or DMSO treatment. DMSO treated spheroplasts were similar to untreated spheroplasts and assembled equatorial actomyosin rings with an average R/S of ~0.86 ± 0.11 (Figure 3.11, panel A and B). Interestingly, we found two classes of contractile actomyosin rings upon swinholide-A treatment. There were ~14% of spheroplasts which formed the contractile actomyosin ring at equatorial regions (Figure 3.11, panel A and B). In the other ~86% of spheroplasts, contractile actomyosin rings assembled at non-equatorial positions after swinholide-A treatment, with an average R/S shifted to ~0.65 ± 0.18 (Figure 3.11, panel A and B). A large number of rings showed an R/S ratio of 0.5 or even less (Figure 3.11, panel A and B).

Previous work performed by Kovar and colleagues proposed that Cdc3 (profilin) antagonizes actin branching and favours actin filament elongation. Profilin mutant *cdc3*-124 is defective in cytokinesis, causing an abnormal F-actin containing contractile ring to form at the restrictive temperature [144, 145]. We therefore attempted to partially compromise the actin polymerization factor Cdc3-profilin in *mid1*-18 *tea1Δ* by creating a triple mutant, and then growing this strain at the semi-restrictive temperature of 33°C. We found that ~87% *mid1*-18 *tea1Δ* *cdc3*-124 spheroplasts assembled non-equatorial rings with an average R/S of ~0.54 ± 0.23 (Figure 3.11, panel C and D). It is likely that the partially compromised Cdc3-profilin slows down actin polymerization, leading to shorter actin filaments, which are then organized into contractile actomyosin rings with higher curvature when compared to *cdc3*+ strains.

Collectively, these experiments suggest that long actin filaments were formed in spheroplasts during actomyosin ring assembly, and that these follow the path of least curvature (i.e. forming around the cell equator) to minimize their elastic bending energy. However, when

shorter actin filaments are generated upon swinholide-A treatment or partially compromising Cdc3p function, this allowed for the assembly of non-equatorial actomyosin rings, presumably because the actin filaments produced in these cells had lengths that were much smaller than the measured persistence length of actin filaments, causing them to behave like stiff rods rather than as an elastic material.

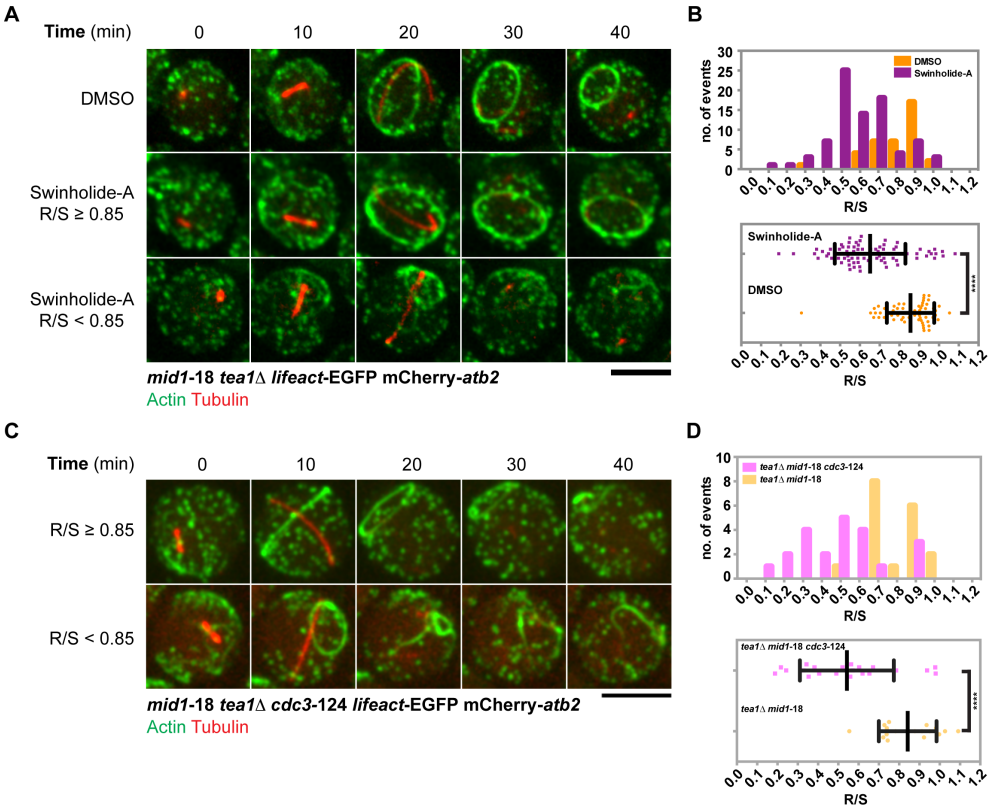

Figure 3.11 Effect of reducing actin filament lengths in *mid1*-18 *tea1Δ* spheroplasts.

(A) *mid1*-18 *tea1Δ* spheroplasts expressing *lifeact*-EGFP (actin) and mCherry-Atb2 (tubulin) were incubated with DMSO or with 10 μM swinholide-A. Top: DMSO control; middle: a ring assembled with a larger circumference; bottom: a ring assembled with a smaller circumference. See also Movie S4.

(B) Top: Distribution of the R/S ratios of spheroplasts incubated with DMSO (n = 62) or with 10 μM swinholide-A (n = 83). Bottom: comparison of the R/S ratios of *mid1*-18 *tea1Δ* spheroplasts incubated with DMSO (n = 62) or with 10 μM swinholide-A (n = 83) (****p < 0.0001).

(C) *mid1*-18 *tea1Δ cdc3*-124 spheroplasts expressing *lifeact*-EGFP (actin) and mCherry-Atb2 (tubulin) were imaged at 33ºC. Top: a ring assembled with a larger circumference; bottom: a ring assembled with a smaller circumference.

(D) Top: Distribution of the R/S ratios of *mid1*-18 *tea1*Δ cdc3-124 spheroplasts (n = 22) and *mid1*-18 *tea1*Δ spheroplasts (n = 18). Bottom: comparison of the R/S ratios of *mid1*-18 *tea1Δ cdc3*-124

spheroplasts (n = 22) and *mid1*-18 *tea1Δ* spheroplasts (n = 18) (****p < 0.0001).

Scale bars = 5 μm. Error bars indicate SD.

3.2.9 Compression of spheroplasts leads to formation of elongated contractile actomyosin ring.

We hypothesized that contractile actomyosin rings would follow the path of minimal curvature during assembly in spheroplasts lacking Mid1p and Tea1p. If this were the case, then compression of spheroplasts would be expected to cause the ring to assemble parallel to the imaging plane and perpendicular to the axis of compression. To test this hypothesis, spheroplasts of *mid1*-18 *tea1Δ* spheroplasts were compressed mechanically on agarose pad with a coverslip, as illustrated in Figure 3.12.

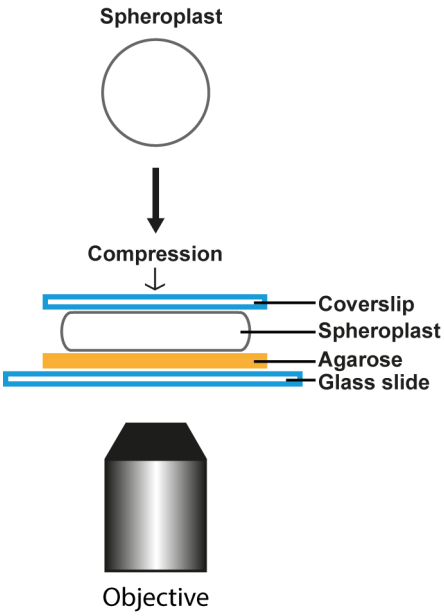

Figure 3.12 Compression of spheroplasts.

A diagram illustrating the compression of spheroplasts by sandwiching and pressing spheroplasts between a coverslip and an agarose pad.

Contractile actomyosin rings in uncompressed spheroplasts demonstrate circular and uniform curvature (Figure 3.13). However, in 28 out of 28 compressed spheroplasts that we imaged actomyosin rings were assembled parallel to the imaging plane and perpendicular to the plane of compression. Further analysis revealed that these rings had large segments of low local curvatures (Figure 3.13).

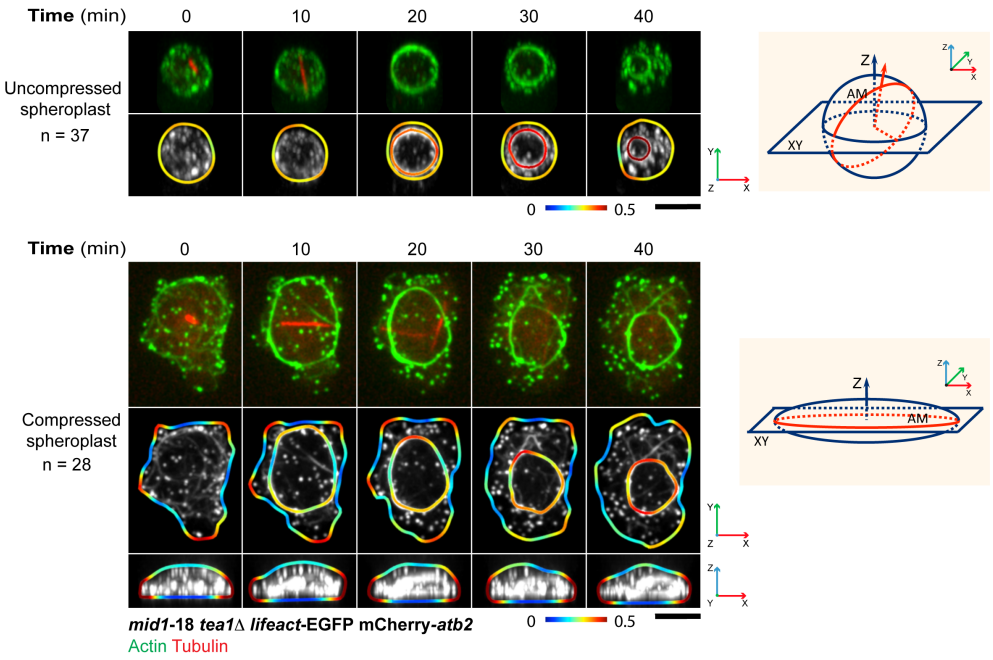

Figure 3.13 Curvature analysis of ring assembly in compressed spheroplasts.

Assembly of rings at the larger cell circumference in compressed *mid1-18 tea1Δ* spheroplasts. The top two panels are uncompressed spheroplasts (n = 37). The bottom three panels are compressed spheroplasts (n = 28). Curvatures of the ring and spheroplast circumferences are colour coded with the rainbow look-up table. For the uncompressed spheroplasts, the image was rotated so that the ring was parallel to the imaging plane for curvature measurement. The projection axes of the displayed images are indicated by the arrows labelled with x-y-z. The two diagrams illustrate the imaging axes. AM, actomyosin ring. (Figure provided by Anton Kamnev)

Scale bars = 5 μm.

3.2.10 Contractileactomyosin rings assemble along the long axis of a *mid1*-18 *tea1Δ* cell.

We wondered if the adoption of the path of least curvature only applied to contractile actomyosin rings in spheroplasts. To test this prediction, we imaged contractile actomyosin rings in rod-shaped *S. pombe mid1*-18 *tea1Δ* cells. Upon entry to mitosis, these cells assembled obround actomyosin rings that spanned the entire length of the cell (Figure 3.14). Our observations established that even in rod-shaped cells, loss of actomyosin ring-positioning factors led to ring assembly along the path of least curvature. This experiment also suggested that the assembly of actomyosin ring parallel to the imaging plane in compressed spheroplasts was not an outcome of the compression. Rather, the assembly of elongated contractile actomyosin rings parallel to the imaging plane is a result of the morphology change in the compressed spheroplasts.

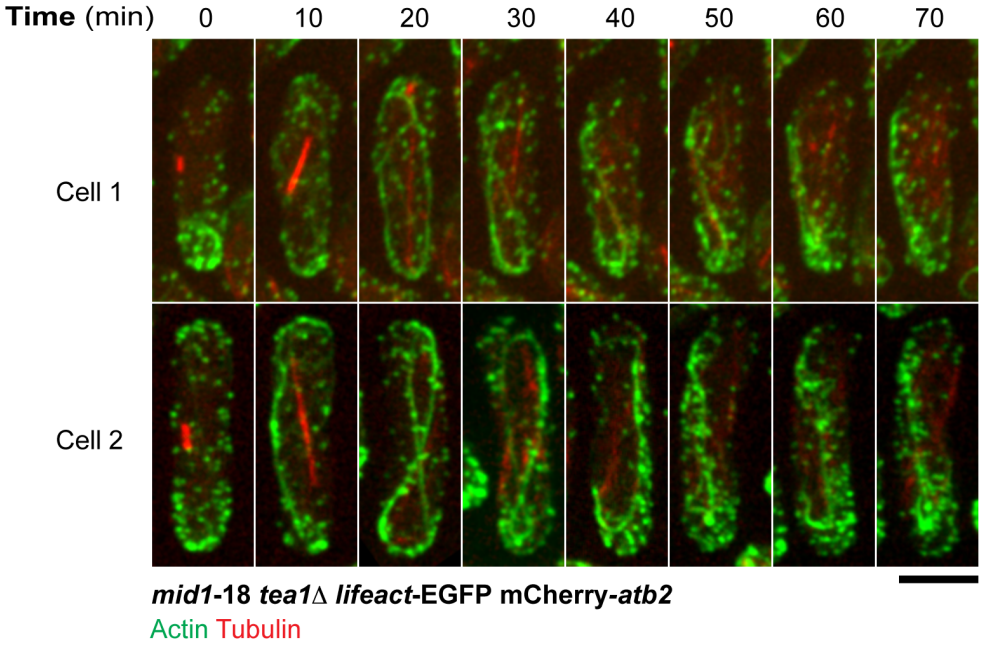

Figure 3.14 Actomyosin ring assembly in *mid1*-18 *tea1Δ* cells.

Actin dynamics in *mid1*-18 *tea1Δ* cells expressing *lifeact*-EGFP and mCherry-Atb2. Two examples are shown.

Scale bars = 5 μm.

Cells lacking Mid1p function and cell-polarity determinant *tea1* have a tendency to form an actomyosin ring that lies parallel to the long axis of cylindrical *S. pombe* cells [81]. This event is lethal to a mitotic cell as the ring will cut across the nuclei during constriction. We speculated that the survivability of the double mutant can be raised in a spherical cell. To test this assumption, we performed UV mutagenesis on *mid1*-18 *tea1Δ* cells to identify mutations that could rescue the viability of the *mid1*-18 *tea1Δ* cells. UV mutagenesis resulted in 185 mutants that could survive in non-permissive condition, and 28 of these mutants were spherical at room temperature.

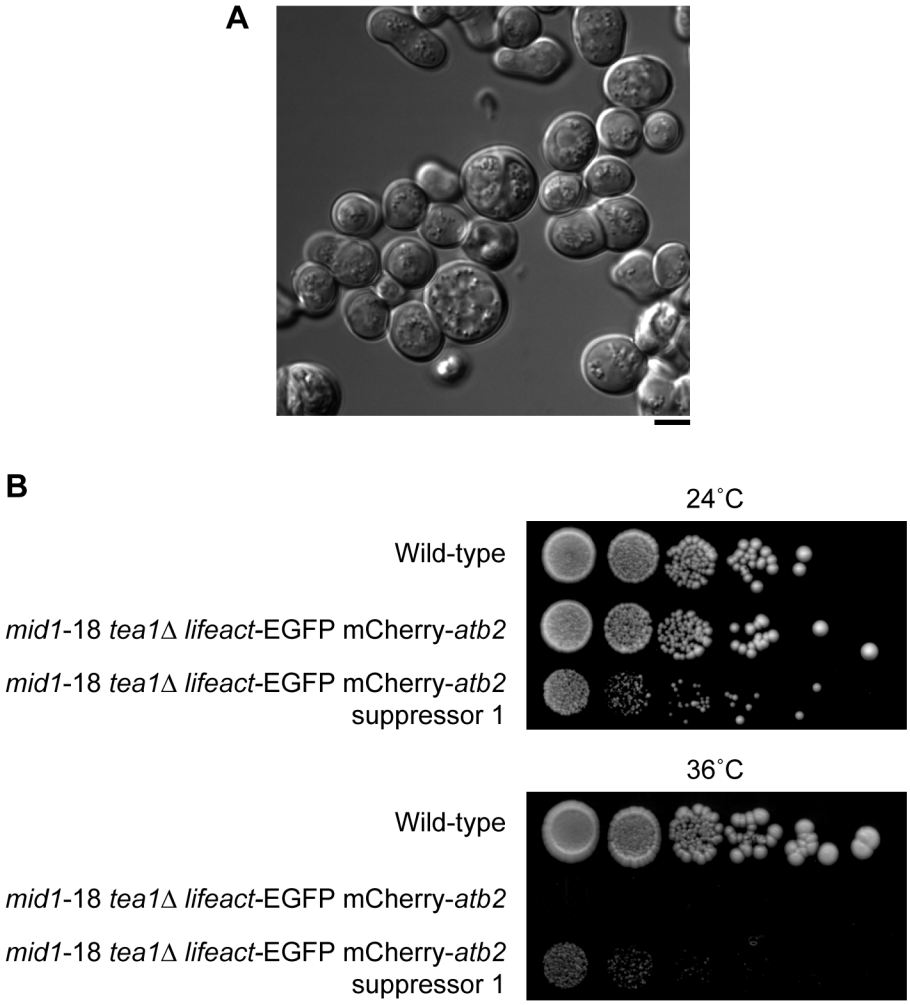

Figure 3.15 Suppressor mutants of mid1-18 *tea1Δ* cells generated by UV mutagenesis.

(A) *mid1*-18 *tea1Δ* suppressor mutant cells at permissive temperature on YEA agar.
(B) Wild-type and *mid1*-18 *tea1Δ* suppressor mutant cells were serially diluted, spotted on two YE agar plates, and incubated at 24°C and 36°C respectively. The *lifeact*-EGFP driven under the *S. pombe* actin promoter was used to label actin filaments.

Scale bar = 5 μm.

3.3 DISCUSSION

3.3.1 The assembly of contractile actomyosin rings favours the path of minimum curvature.

In *S. pombe*, the contractile actomyosin ring assembles at the medial region of the cylindrical cell to produce two daughter cells, and the precise positioning of the ring helps to ensure the even distribution of genetic material between the two daughter cells, avoiding aneuploidy and daughter cell lysis. Our experiments showed that when a cell is lacking the functions of Mid1p and Tea1p, the ring assembled along the long axis of the cylindrical cell. Huang and colleagues' work also identified *mid1*-18 *tea1Δ* cells with septa that span the long axis [81].

Studies have shown that single actin filaments have a persistence length of 5-18μm [99-102]. Recent *in vitro* experiments provided insights into actin filament properties, where it has been suggested that actin filaments favour aligning at the long axis in a rectangular confined space to reduce the bending energy in these elastic structures [146]. Similarly, actin filaments orient near the equator in a spherical confined space due to their structural rigidity [147]. These studies could provide an insight as to why the actomyosin rings in untreated and DMSO-treated spheroplasts assembled at the equatorial regions in our experiments. Severing of actin filaments by Swinholide-A, or inhibiting their polymerisation through the use of profilin mutants, caused actomyosin rings to assemble at non-equatorial regions. Since these treatments likely result in shorter actin filaments being produced, and these shorter filaments are more likely to behave like stiff rods, these treatments may allow actomyosin rings to assemble at regions of

higher curvature within spheroplasts. Therefore, our results are consistent with these studies, indicating actin properties could be a key element in determining ring positioning in the absence of additional positioning cues.

3.3.2 Actin properties in actomyosin ring assembly in the absence of spatial cues.

In rod-shaped cells lacking *mid1* and *tea1* functions, actomyosin rings are assembled along the long axis. This led us to hypothesize that the absence of *mid1* and the tip-complex led to actomyosin rings following the path of least curvature, where in a rod-shaped cell, is the long axis, while in a sphere, the equator. It is likely that due to the preference of actin filaments and bundles to be as straight as possible within the persistence length considerations. Actin filaments have a persistence length of >10μm [148]. Since actomyosin rings in *S. pombe* cells are composed of actin filaments of ~600nm in length, shorter filaments is likely assembled along the short axis with ease [149, 150]. We speculate the possibility of Mid1p and/or cortical nodes do not only ensure medial assembly of actin filaments, but also contribute to ensuring that actin filaments remain short to be organized along the short axis of the cell [151]. In the *mid1* mutant cells, and in wild-type and *mid1* spheroplasts, it can happen that actin filaments are longer, resulting in spontaneous organization along the equator in a path of least curvature. We found that generating shorter filaments with pharmacological means promotes non-equatorial ring assembly in spheroplasts, as shorter actin filaments may become easily packed in smaller and more curved actomyosin rings.

3.3.3 Mid1p and Tea1p functions suppress the default contractile actomyosin ring positioning.

In a spheroplast lacking Mid1p and Tea1p functions, the ring assembles at the equatorial region. Our observations indicate that these contractile actomyosin rings preferentially form along the path of minimum curvature, which is lethal to a cell. In a cylindrical *S. pombe* lacking Mid1p and Tea1p function, we observed abnormal actomyosin ring assembly that spans the long axis of the cell, which complements the work of Huang and colleagues [81]. In addition to this, they also observed tip-anchored membrane invaginations and septa [81]. Due to the aberrant positioning of the contractile actomyosin ring, the *mid1*-18 *tea1Δ* cells are inviable at their restrictive temperature. These results suggest that Mid1p acts in conjunction with Tea1p, which plays a role as a negative cue to prevent retention of the contractile actomyosin ring and septum assembly at the cell ends [81]. These cues prevent the formation of the actomyosin ring along the long axis of the cells, and instead confine it to the medial region, and to being perpendicular to the long axis.

Systematic studies have been performed to identify the functions of different Mid1 domains. Mid1 interacts with the plasma membrane through its C-terminal region, which is made up of a PH domain and an anillin-homology domain (AHD) [44]. During the course of our attempts to generate *mid1*-18 *tea1Δ* suppressor mutants, a library of strains that have acquired mutations in *mid1* was collected. Sequencing of the *mid1* locus in these mutants could help us to gain more insights into the structure-function relationship within Mid1p.

4. CYTOKINESIS IN THE ABSENCE OF CELL WALL

4.1 INTRODUCTION

Cell separation takes place after mitosis and cytofission. This process requires the formation of division septum, which is composed mainly of the same types of polysaccharides that constitute the cell wall [152-154]. In animal cells and yeast, formation of septum involves two processes – assembly of contractile actomyosin ring and deposition of septum materials [155, 156]. Ring contraction drives membrane ingression and coordinates with the septum assembly machinery to deposit cell wall materials at the division site.

The physical separation of two daughter cells involves membrane abscission at division site as well as break-down of septum. Advanced imaging and biochemical methods suggest endosomal sorting complex required for transport (ESCRT) components participates in final membrane abscission. Yeast studies have reported that the ESCRT components accumulate to endosomal membranes where they mediate protein sorting, membrane remodeling and fission at the appropriate timing [157-161].

Aiding cell separation of fission yeasts are primary septum and septum edge materials. The Cps1p is responsible for synthesis of the major component of cell wall septum, 1,3-β-glucan and Mok1p is responsible for 1,3-α-glucan [152, 154, 162]. The cell wall is not solely important in maintaining cell shape and polarity, but also act as a key player in ensuring complete daughter cell separation during division [122]. Treatment of 1,3-α-glucan renders the rod-shaped fission yeast

round, known as a protoplast [163]. The dissolution of primary septum and septum edge involves the 1,3-β-glucanase, Eng1p and 1,3-α-glucanase Agn1p to breakdown the β-glucan and α-glucan respectively [130, 132]. Complete breakdown of septum and its surrounding cell wall material will enable the daughter cells to detach from each other.

Whether the extracellular glycan matrix has any influence on the actomyosin ring contraction apart from its roles in ring stability during cytokinesis has not been examined closely. In this study, we used the thermosensitive allele of 1,3-β-glucan synthase, *cps1*-191 to address this question. The *cps1*-191 mutant is defective in β-glucan and septum synthesis and arrests with a non-contracting actomyosin ring at the non-permissive temperature [127]. In this chapter, we report that weakening of the extracellular glycan matrix in *cps1*-191 mutant at the non-permissive temperature enabled actomyosin ring contraction and membrane ingression.

4.2 RESULTS

4.2.1 Lowering turgor pressure does not rescue the lethality of *cps1*-191 mutants.

Cps1-191 is a cytokinetic mutant allele isolated by Liu *et al*. in 1999. Here they found that this mutant was temperature-sensitive, hence showing a phenotype in restrictive condition at 36°C. Cell proliferation was retarded and unable to form a division septum after incubation for 4 hours at restrictive temperature. Although actomyosin rings assemble as usual in the mutants, ring constriction was defective. Our experiments showed that the *cps1*-191 cells assemble actomyosin rings that do not constrict in restrictive temperature (Figure 4.1, panel A). In some cases, the cells form a bump at close proximity the cell tips and

lysed later (Figure 4.1, panel B). Previous work has proposed that actomyosin ring may not be able to overcome the high intracellular turgor pressure during cytokinesis, and β-glucan synthesis is needed at the division site. We asked if ring constriction in *cps1*-191 mutants is inhibited by the turgor pressure. We cultured the mutant cells in a low turgor condition, a medium containing 0.8M sorbitol and added 2-deoxyglucose to this culture to prevent further glucan synthesis at the division site and other locations in the cell. Even so, the change in condition did not increase the number of cytokinetic events, and phenotypically these *cps1*-191 cells resembled those grown with normal turgor pressure (Figure 4.1, panel C and D). Hence, these results showed that the inability of ring constriction in *cps1*-191 cells cannot be suppressed by a decreased turgor pressure.

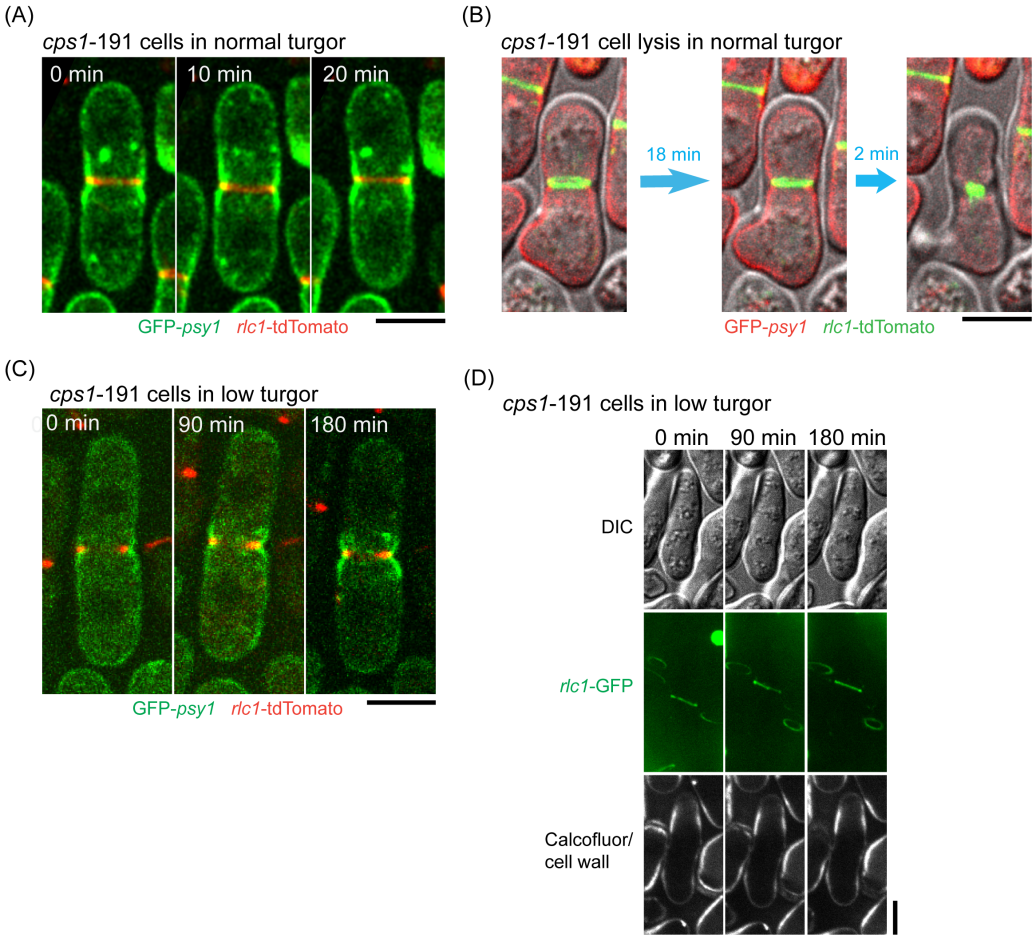

Figure 4.1 Lowering down turgor pressure does not allow cell membrane ingression in *cps1* mutant cells. (Work done in collaboration with Ting Gang Chew)

(A) The *cps1*-191 GFP-*psy1* *rlc1*-tdTomato cells were cultured at 36°C for 6.5 hours and continued to image at 36°C.
(B) Some *cps1*-191 GFP-*psy1* *rlc1*-tdTomato cells lysed after more than 6.5 hours of incubation at the restrictive temperature.
(C) The *cps1*-191 GFP-*psy1* *rlc1*-tdTomato cells were cultured at the restrictive temperature for 6.5 hours and continued to image at 36°C in medium containing 0.8 M sorbitol to lower down the turgor pressure.
(D) The *cps1*-191 GFP-*psy1* *rlc1*-tdTomato cells were cultured at the restrictive temperature for 6.5 hours and continued to image at 36°C in medium containing 0.8 M sorbitol. Calcofluor was used to stain the cell wall.

Scale bars = 5 μm.

4.2.2 Weakening of cell wall allows ring contraction and cell membrane ingression

We sought to examine the possibility that the extracellular glycan matrix are hindering ring constriction and membrane ingression in *cps1*-191 mutants. The Cps1p is a transmembrane protein that links actomyosin ring underneath the cell membrane to the extracellular glycan matrix. Therefore we considered it was possible that in the absence of division septum synthesis (and thereby cell wall remodelling), the actomyosin rings are anchored to the inactive *cps1*-191 gene-product at the division site. To test to this hypothesis, we treated the *cps1*-191 cells (expressing the regulatory light chain of myosin tagged with fluorescent protein tdTomato) with cell wall lysing enzymes to weaken the existing extracellular glycan matrix (Figure 4.2). On top of that we further blocked new cell wall and septum formation by adding 2-deoxyglucose to the culture medium. 2-deoxyglucose generated UDP-linked 2-deoxyglucose which is incorporated into the cell wall β-glucan chain, which renders the structures less stable and more susceptible to breakdown by glucanase actions [164].

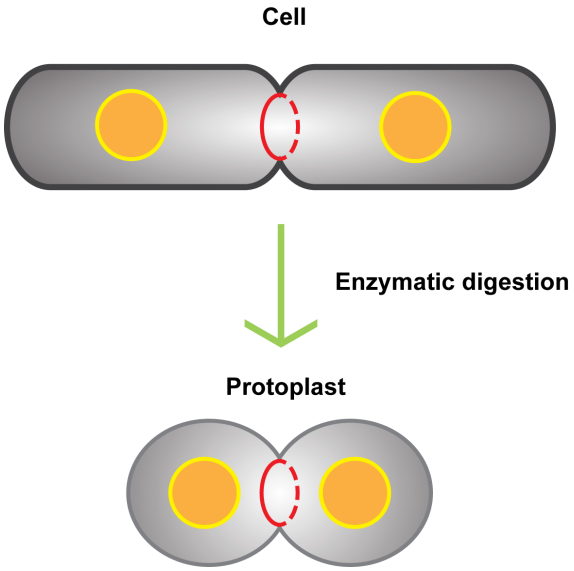

Figure 4.2 Yeast protoplast transformation.

Cells were treated with lysing enzyme to hydrolyze the cell wall β-glucan. Dividing cells at the point of treatment acquire a dumbbell shape.

Remarkably, fluorescence microscopy showed that upon weakening of the cell wall, myosin rings in *cps1*-191 mutant underwent contraction coupled with membrane ingression (Figure 4.3, panel A; GFP-tagged Syntaxin-like protein Psy1 was used as a cell membrane marker; n = 6 protoplasts). Contracting actin rings labelled with the *lifeact*-mCherry were also detected in the *cps1*191 mutant upon treatment of lysing enzyme on the cell wall. This suggested that the actomyosin rings were driving the contraction and membrane ingression (Figure 4.3, panel B, n = 5 protoplasts). The dividing protoplast appeared was two lobes and bear resemblance to certain animal cell types. These protoplasts generally divided non-medially into two, and the rings contracted at a much lower rate (0.061 +/- 0.212 μm/s, $n_{protoplast}$ = 8) compared to wild-type cells (0.299 +/- 0.059 μm/s, n_{cell} = 14,)

(Figure 4.3, panel C). We frequently observed the rings contracted till mid-phase of division and disassembled before completion of cytokinesis. The protoplasts then progressed to divide into two entities (Figure 4.3, panel A and B; bottom panels respectively).

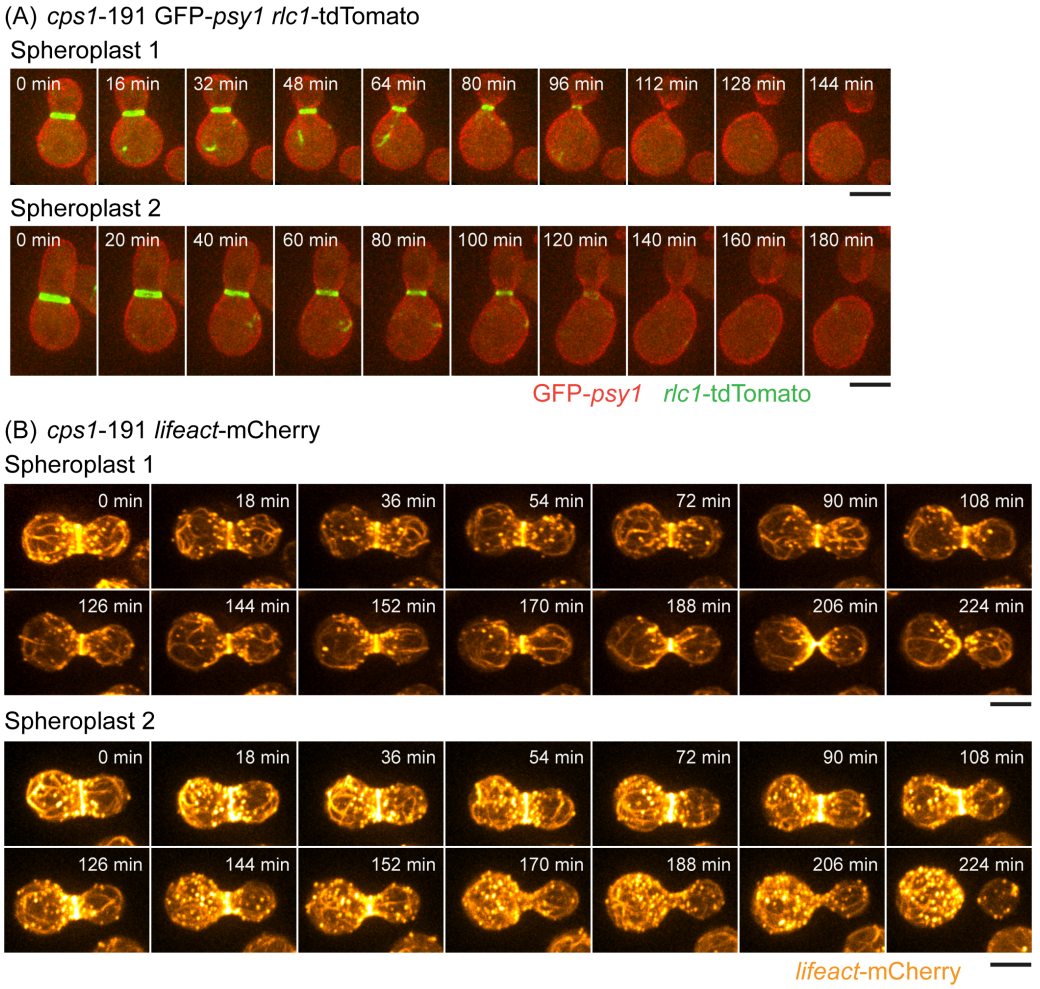

Figure 4.3 Weakening of cell wall allows ring contraction and cell membrane ingression. (Work done in collaboration with Ting Gang Chew)

(A) Two examples of *cps1*-191 protoplasts underwent cytofission at 36°C. The *cps1*-191 GFP-*psy1 rlc1*-tdTomato cells were cultured at 36°C for 6.5 hours, processed into protoplasts, and recovered for 1 hour at 36°C prior to imaging.
(B) Two examples of *cps1*-191 protoplasts expressing *lifeact*-mCherry underwent cytofission at 36°C. The *cps1*-191 GFP-*psy1 lifeact*-mCherry cells were cultured at 36°C for 6.5 hours, processed into protoplasts, and recovered for 1 hour at 36°C prior to imaging.
(C) Quantification of the rate of ring contraction in wild type cells and cps1-191 protoplasts undergoing cytofission.

Scale bars = 5 μm. Error bars indicate SD.

4.2.3 Segregation of nuclei to daughter protoplasts is abnormal

To gain insight on the segregation of daughter nuclei in these mutant protoplasts, we generated *cps1*-191 mutants with histone gene tagged with GFP. We discovered that the segregation of daughter nuclei here was in most of the cases not coordinated with the cytokinesis. Likely a result of non-medial division, some daughter protoplasts acquired multiple nuclei or cleaved nuclei (Figure 4.4). The *cps1*-191 mutant protoplast division was morphologically distinct compared to normal fission yeast cell division. Rather, the process was mimicking the morphological modification in animal cells during division. Hence we have called this type of division as cytofission.

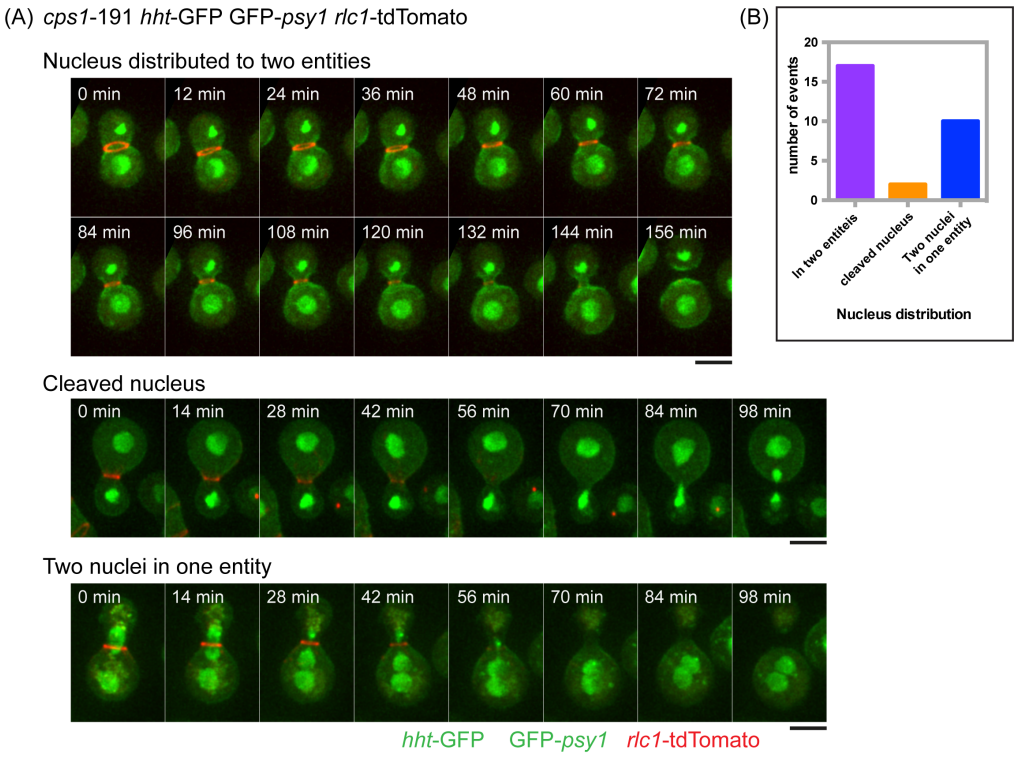

Figure 4.4 Abnormal nuclei segregation in daughter protoplasts.

(A) Top panel: Dividing c*ps1*-191 protoplasts exhibiting nucleus distributed to two daughter protoplasts (n = 17). Middle panel: *cps1*-191 protoplasts showed uneven nucleus segregation - cleaved a nucleus while dividing (n = 2). Bottom panel: Dividing c*ps1*-191 protoplasts showed uneven nucleus segregation – both daughter nuclei in one of the daughter protoplast only (n = 10).

(B) Quantification of number of spheroplasts with normal and abnormal distribution of nuclei.

Scale bars = 5 μm.

4.2.4 Protoplasts achieved cytofission with significantly reduced amount of cell wall

In order to examine the extracellular glycan matrix in cells undergoing cytofission, we added the CW (a division septum-specific fluorochrome) to a mixture of cells and protoplasts culture. The staining revealed that the division site of *cps1*-191 protoplasts in the process of cytofission contained significantly reduced deposition of β-glucan materials (Figure 4.5, panel A). Figure 4.5 panel B demonstrates further study with the high-resolution scanning electron microscopy showed that the β-glucan fibrils commonly present at the division site of fission yeast was largely absent in the *cps1*-191 protoplasts in the midst of cytofission. Collectively, these data revealed that weakening of cell wall in *cps1*-191 cells at non-permissive temperature facilitates a novel cytofission event that leads to division of one protoplast into two in the absence of detectable division-septum growth. The extracellular glycan matrix anchored to the actomyosin rings could negatively regulate the ring contraction and membrane ingression.

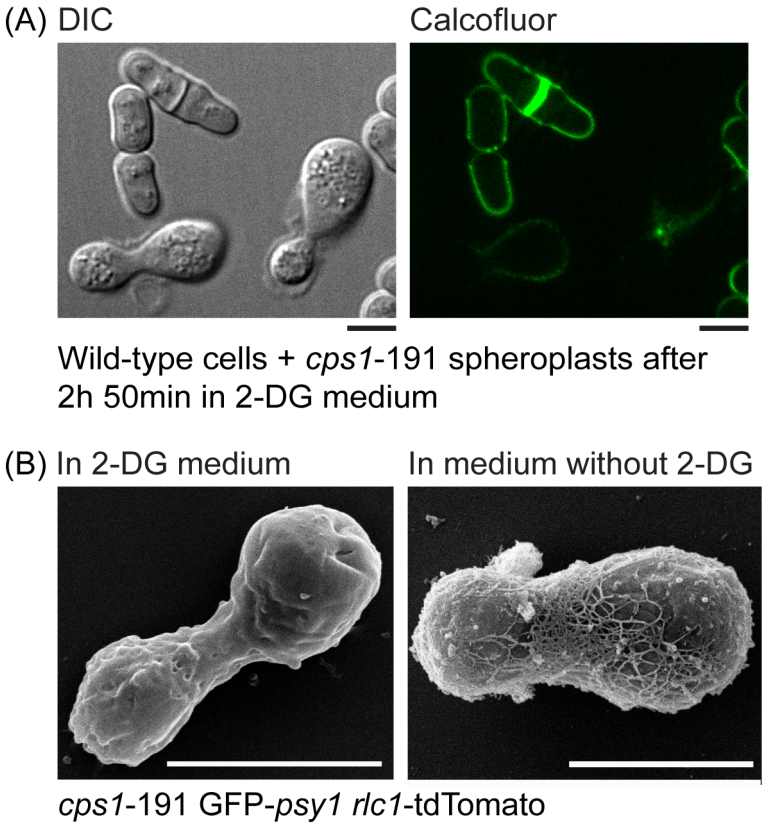

Figure 4.5 Cytofission event takes place with significantly reduced cell wall in protoplasts. (Work done in collaboration with Ting Gang Chew)

(A) The wild type cells and *cps1*-191 GFP-*psy1 rlc1*-tdTomato protoplasts were stained with the calcofluor dye.
(B) Electron micrographs of *cps1*-191 GFP-*psy1 rlc1*-tdTomato protoplasts regenerated in medium with or without 2-DG. (Figure provided by Masako Osumi)

Scale bars = 5 μm.

4.2.5 Separation of *cps1* mutant protoplasts does not require α-glucan synthase

A reduction of β-glucan may triggered the cell to respond with an increased amount of α-glucan in the cell wall of fission yeast. We asked if the cytofission of *cps1*-191 protoplasts were due to the elevated synthesis of α-glucan at the division site. To test this hypothesis, we generated the *cps1*-191 *mok1*-664 double mutant protoplasts containing the thermosensitive alleles of both α- and β-glucan synthases. We then imaged the myosin rings and cell membrane of this double mutant protoplasts at the 36˚C in the presence of 2-DG. Similar to the *cps1*-191 protoplast, the *cps1*-191 *mok1*-664 double mutant protoplasts underwent cytofission (Figure 4.6, n = 8), suggesting that α-glucan and β-glucan synthesis did not contribute significantly to the cytofission event.

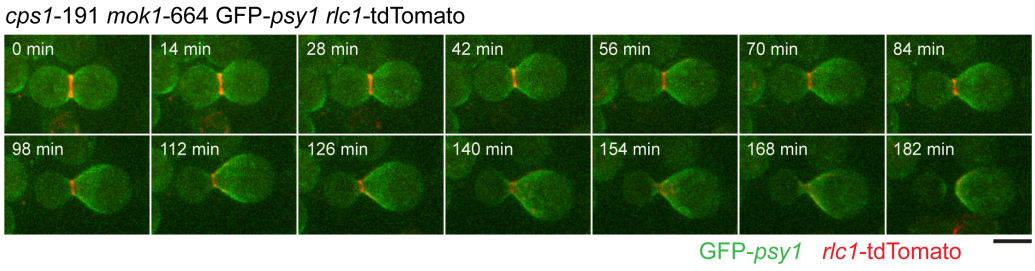

Figure 4.6 Separation of *cps1* mutant protoplasts does not require α-glucan synthase.

An example of *cps1*-191 *mok1*-664 GFP-*psy1* *rlc1*-tdTomato protoplasts underwent cytofission.

Scale bars = 5 μm.

4.2.6 Separation of *cps1* mutant protoplasts does not require exoglucanases

Normal fission yeast cells that just complete ring contraction and membrane ingression are not entirely separated until the digestion of division septum connecting the two newly-divided cells [162]. This process is achieved in fission yeast through the action of exoglucanases [129, 130, 132]. If trace amounts of division septum had been deposited during ring contraction, we could expect the proteins involved in the separation of fission yeast cells are also involved in the cytofission. To test this proposition, we constructed double mutant protoplasts of *cps1*-191 lacking the exoglucanases *agn1* (α-glucanase) and *eng1* (β-glucanase) respectively. The results suggested that, even though cytofission events lead to the complete separation of protoplasts, the *cps1*-191 mutant does not require the break-down of cell wall materials by exoglucanases for cytofission (Figure 4.7).

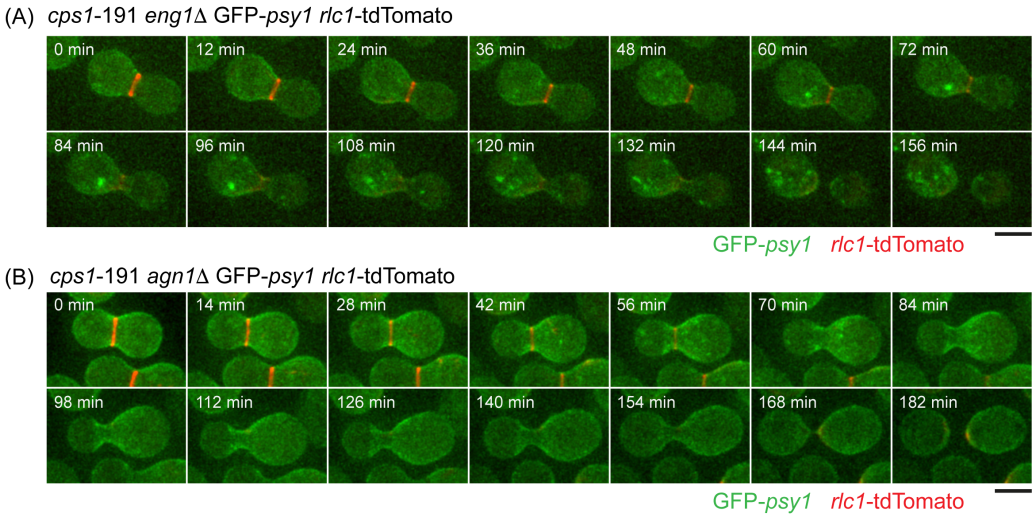

Figure 4.7 Separation of *cps1* mutant protoplasts does not require exoglucanases.

(A) An example of *cps1*-191 *eng1*Δ GFP-*psy1 rlc1*-tdTomato protoplasts underwent cytofission.
(B) An example of *cps1*-191 *agn1*Δ GFP-*psy1 rlc1*-tdTomato protoplasts underwent cytofission.

Scale bars = 5 μm.

4.2.7 Separation of *cps1* mutant protoplasts does not require ESCRT proteins like Vps20 and Vps4

In ~70% of the *cps1*-191 protoplasts (40 out of 57 protoplasts) that underwent cytofission, the rings contracted till mid-phase of division and disassembled before division into two entities. We proceeded to test if the ESCRT abscission complex was involved in the cytofission by removing the ESCRT proteins Vps20 and Vps4 in the *cps1*-191 protoplasts. The *cps1*-191 *vps20Δ and cps1*-191 *vps4Δ* mutant protoplasts underwent cytofission resembling the cytofission event in *cps1*-191 single mutant protoplasts (Figure 4.8). This result suggested that ESCRT abscission complex is unlikely to play a major role in the completion of cytofission in protoplasts.

(A) *cps1*-191 *vps20*Δ GFP-*psy1 rlc1*-tdTomato

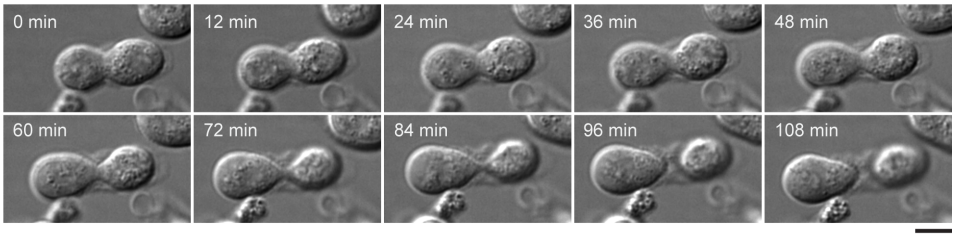

(B) *cps1*-191 *vps4*Δ GFP-*psy1 rlc1*-tdTomato

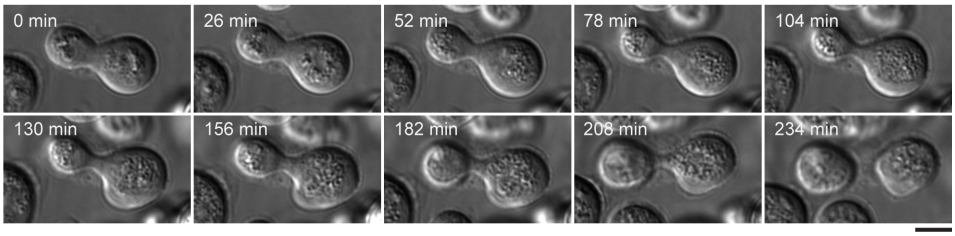

Figure 4.8 Separation of *cps1* mutant protoplasts does not require ESCRT proteins like Vps20 and Vps4. (Work done in collaboration with Ting Gang Chew)

(A) An example of *cps1*-191 *vps20Δ* GFP-*psy1 rlc1*-tdTomato protoplasts underwent cytofission.
(B) An example of *cps1*-191 *vps4Δ* GFP-*psy1 rlc1*-tdTomato protoplasts underwent cytofission.

Scale bars = 5 μm.

4.2.8 Separation of *cps1* mutant protoplasts requires actomyosin ring

Previous studies suggested under certain circumstances, some eukaryotic cells are able to divide without an actomyosin ring [165-167]. To address whether the cytofission event was caused by contraction of the actomyosin ring, we attempted to perturb the functions of rings using the Latrunculin-A (Lat-A) to block actin polymerization [168, 169]. The *cps1*-191 cells treated with DMSO underwent ring contraction, membrane ingression and lastly completed ingression as previous

experiments (Figure 4.9, panel A; n = 7 protoplasts). In contrast, the pre-assembled ring in *cps1*-191 protoplasts treated with Lat-A underwent disassembly and failed to divide into two daughter protoplasts. Remarkably, the smaller entity retracted into the bigger entity, presumably due to the imbalance intracellular pressures (Figure 4.9, panel B; n = 8 protoplasts).

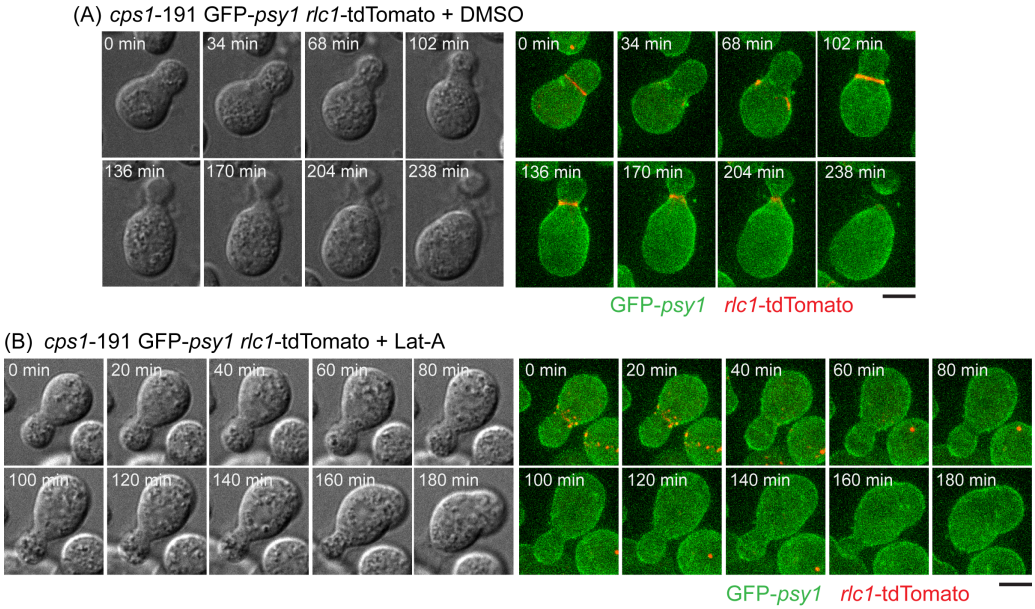

Figure 4.9 Separation of *cps1* mutant protoplasts requires actin rings. (Work done in collaboration with Ting Gang Chew)

(A) The *cps1*-191 GFP-*psy1 rlc1*-tdTomato protoplasts underwent cytofission in the presence of DMSO. Left panel shows the DIC images; right panel shows the fluorescence micrographs.
(B) The *cps1*-191 GFP-*psy1 rlc1*-tdTomato protoplasts were incubated with 150 μM Lat-A. Left panel shows the DIC images; right panel shows the fluorescence micrographs.

Scale bars = 5 μm.

Subsequently we perturbed the myosin component of actomyosin rings by generating a *cps1*-191 mutant lacking the myosin regulatory light chain, *rlc1*. Previous work has shown that the cells lacking *rlc1* (*rlc1*Δ) becomes cold-sensitive and could not undergo cytokinesis at 19˚C [170-172]. Yet at 32˚C the *rlc1*Δ cells assembled an intact actomyosin ring that contracts as usual [170]. We observed that the *rlc1*Δ cells are capable of cell division at 36˚C (Figure 4.10, panel A, n = 23 cells). To obtain insights into the essentiality of actomyosin ring functions in cytofission we imaged the *cps1*-191 *rlc1*Δ double mutant protoplasts at 36˚C. If the actomyosin ring was essential in driving cytofission, the absence of *rlc1* might render the cells with weakened cell wall unable to undergo cytofission at the high temperature, which is normally permissive for *rlc1*Δ cells alone [170]. Similar to the Lat-A experimental findings, the double mutant *cps1*-191 *rlc1*Δ protoplasts did not undergo ring contraction at 36˚C (Figure 4.10, panel B; n = 28 protoplasts), whereas the single mutant of *cps1*-191 could undergo cytofission.

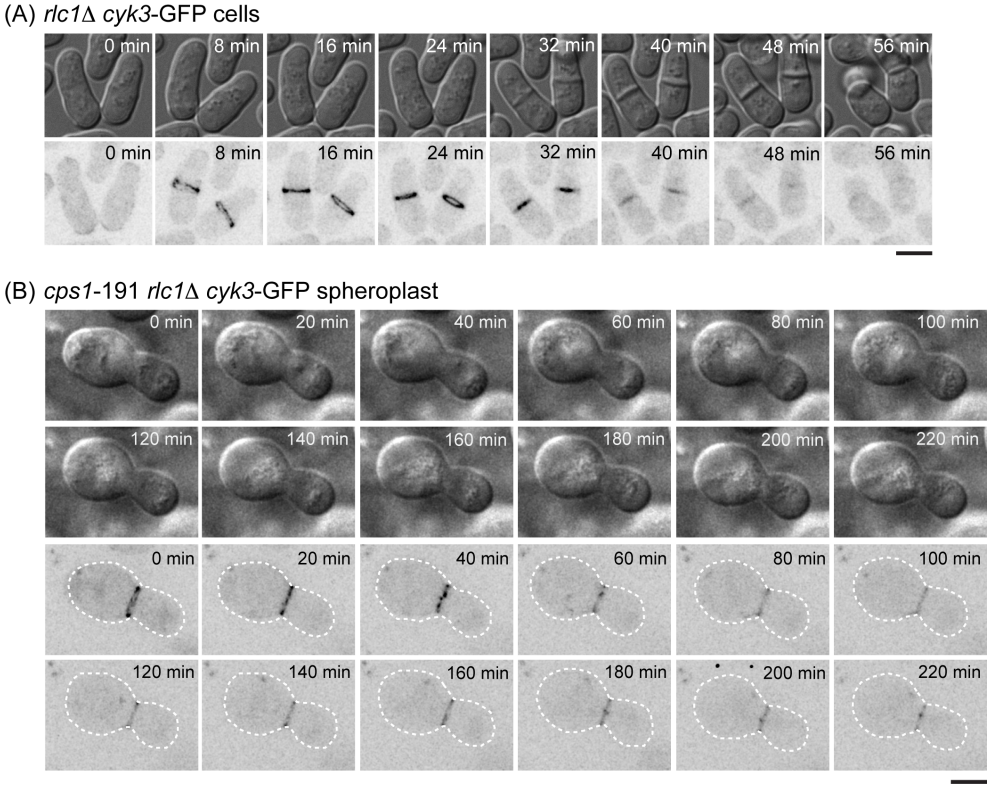

Figure 4.10 Separation of *cps1* mutant protoplasts requires myosin rings. (Work done in collaboration with Ting Gang Chew)

(A) The *rlc1*Δ *cyk3*-GFP cells underwent cytokinesis at 36°C. The *rlc1*Δ *cyk3*-GFP cells were cultured at 36°C for 6.5 hours, washed with protoplasting buffers without lysing and lytic enzymes, and then recovered in minimal medium containing sorbitol prior to imaging at 36°C. Top panel shows the DIC images; bottom panel shows the fluorescence micrographs.

(B) The *rlc1*Δ *cyk3*-GFP protoplasts failed to undergo cytofission at 36°C. The *rlc1*Δ *cyk3*-GFP cells were cultured at 36°C for 6.5 hours, processed into protoplasts, and then recovered in minimal medium containing sorbitol prior to imaging at 36°C. Top panel shows the DIC images; bottom panel shows the fluorescence micrographs.

Scale bars = 5 μm.

Next, we tested whether targeted membrane deposition at the division site promotes actomyosin ring contraction in cytofission. When we inhibited the vesicular trafficking across the endomembrane system with brefeldin A in the *cps1*-191 protoplasts, the myosin rings were not able to contract to drive cytofission events (Figure 4.11). Our observation suggested that addition of cell membrane via targeted membrane trafficking at the division site is required to enable cytofission.

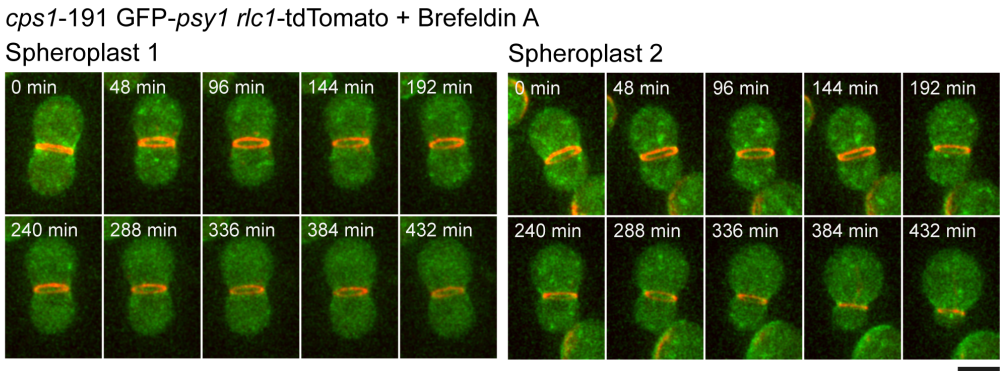

Figure 4.11 Targeted membrane trafficking is required for cytofission events.

75μM brefeldin A was added in to the culture medium with protoplasts before time-lapse imaging begin. The *cps1*-191 GFP-*psy1 rlc1*-tdTomato protoplasts failed to undergo cytofission in the presence of 75 μM brefeldin A.

Scale bar = 5 μm.

4.3 DISCUSSION

4.3.1 Cell membrane ingression is not affected by turgor pressure.

Yeast cell has high internal turgor pressure that enables them to inflate the cell wall, shape the cell and grow in the environment. The turgor pressure, however, is thought to oppose the plasma membrane invagination for various processes including endocytosis and cell division [165, 173]. Cell wall helps to maintain the cell's turgor and cell shape. It was reported that defects in cell wall integrity can sometimes be compensated for by increasing osmolarity of the growth media, as an increase in the environment osmolarity could decrease the turgor pressure in cells [174]. *mok1* mutant cells were able to form colonies on YPD media supplemented with 1.2M sorbitol at non-permissive temperature [128]. However, our observation of *cps1*-191 mutant at permissive temperature showed that an increase in the osmolarity of growth media did not suppress the mutant phenotype where the actomyosin ring were not capable of contracting, subsequently unable to drive membrane ingression. This observation suggests that lowering the turgor pressure is not sufficient to promote cell membrane ingression and actomyosin ring contraction in the β-glucan synthase mutant.

4.3.2 Weakening of cell wall in combination with lowered turgor pressure allow ring contraction and cell membrane ingression.

A previous work done by Proctor *et al.* analysed *cps1*-191 mutants and reported that a defect in division-septum formation caused the failure of membrane ingression in the mutant [165]. They also proposed that the high intracellular turgor pressure prevents actomyosin ring contraction in fission yeast [165]. Our experiments showed that the

actomyosin ring of a *cps1*-191 mutant cell could not drive membrane ingression that leads to cytofission. In some cases the cell lysed. Increasing the surrounding media osmolarity (lowering turgor pressure in cell) could not rescue the phenotype. However, lowering turgor pressure in combination with weakened cell wall, *cps1*-191 mutant protoplasts are able to achieve ring contraction and eventually result in cytofission. This observation is consistent with previous studies on yeast protoplasts. Jochova and colleagues' work showed that when cell wall regeneration was not inhibited, the actomyosin rings of *S. pombe* protoplast revealed only shallow invaginations [175].

A recent study of zebrafish epicardial cells in the heart explants shows the cell-ECM adhesions at the division site and traction forces at the cytokinetic ring inhibit cytokinesis. An early biophysical study also detected a large traction force at the cleavage furrow of the fibroblast cells cultured on an elastic substrate, suggesting an interaction of cytokinetic machinery and ECM. When the cell-ECM adhesion is enhanced during mitosis, the cleavage furrow ingression is inhibited in the epithelial cells. Consistently, we showed that the extracellular glycan matrix inhibits actomyosin ring contraction in the absence of cell wall remodelling and division septum synthesis. Weakening of the extracellular glycan matrix, presumably mimicking a decreased cell-ECM adhesion, has enabled cytofission events.

The slow contraction of actomyosin ring observed in the *cps1*-191 protoplasts agrees with the work of O'Shaughnessy and colleagues, who have proposed that the rate of cytokinesis is dependent on the rate of septum synthesis [176].

4.3.3 The essentiality of actomyosin ring in *cps1* mutant protoplasts fission.

It has been shown that *rlc1*Δ mutants are cold-sensitive – no actomyosin ring assembly and colony growth at 19°C [170]. *rlc1* gene is not essential for cell division or spore germination at up to 32°C [170, 171]. We further search for evidence of rlc1p essentiality at non-permissive temperature. We found that at 36°C, the actomyosin ring of *rlc1*Δ cells disassembled without contracting. We then tried to address this question with *cps1*-191 protoplasts, since they are capable of actomyosin ring contraction that resulted in cytofission. We found that *cps1*-191 *rlc1*Δ double mutant protoplasts are unable to carry out ring contraction. We therefore propose that *rlc1* gene is essential for cytofission in protoplasts are restrictive temperature.

4.3.4 Plasma membrane invagination plays a part in complete cell separation of protoplasts.

Consistent with previous study by Dekker and colleagues, absence of exoglucanases Eng1p and Agn1p do not inhibit cell separation [130]. Nonetheless we observed cytofission after the disassembly of actomyosin ring in protoplasts. Ruling out the cell wall factors, we looked into final membrane abscission's role in complete seperaction of protoplasts. Genetics approach demonstrated that cytofission event in *cps1*-191 protoplasts is independent of membrane remodeling function by ESCRT complex. However, chemical approache of treating the *cps1*-191 mutant protoplasts with brefeldin A inhibited actomyosin ring contraction. This suggests that plasma membrane invagination coupled with ring contraction is important for protoplast cytofission.

5. CONCLUSION AND FUTURE DIRECTIONS

This thesis explored the first principles governing the localization of cytokinetic actomyosin ring, as well as the role of actomyosin ring to drive membrane ingression in *S. pombe*.

It has been known that cell geometry, cell wall and cytokinetic spatial cues mediate the localization of the actomyosin ring. In first part of thesis, we firstly attempted to search for other possible factors that contribute to division site placement. We perturbed all three mentioned factors by generating spheroplasts, as the cylindrical fission yeast cell rounded up after cell wall digestion. We found that the actomyosin ring consistently assembled at the equatorial region of the spheroplast. As we visualized the ring structures with fluorescent tags, we confirmed that tagging the actin structures and myosin regulatory light chain in spheroplasts did not lead to observable cytokinetic defects in spheroplasts. Besides that, we observed equatorial assembly of actomyosin ring in spheroplasts of *mid1* and *tea1* mutants to further confirm that the gene functions are not contributing to the phenomenon.

Remarkably, cells lacking *mid1* and *tea1* functions assembled the actomyosin ring in the long axis, which is lethal to a cell. Treatment of spheroplasts with pharmacological agents generated shorter actin filaments and promoted ring assembly at non-equatorial regions of spheroplasts. Mechanically compressing spheroplasts led to ring perpendicular to the direction of compress. These results further implicates in the absence of *mid1* and *tea1* functions, properties of actin filaments is a major determinant of the positioning of ring assembly. In a cell, *mid1* and *tea1* play a role to promote actomyosin ring assembly with shorter actin filaments at the medial region of a cylindrical cell. With

UV-mutagenesis we were able to isolate *mid1*-18 *tea1Δ* suppressor mutants that became spherical and were viable in non-permissive temperature. More investigations could be done on *mid1* locus to identify *mid1* mutants that could rescue its known defects.

This study implicates the role of the mechanical properties of actin in regulating actomyosin ring localization. To further investigate the dynamics during the assembly of rings in the absence of spatial cues, direct measurements of actin dynamics in rings need to be performed. However, while GFP-labeled actin filaments can be successfully incorporated into actin filaments mediated by the Arp2/3 complex in actin patches, it cannot be incorporated into the actin filaments of contractile rings, which are nucleated by formins (Chen et al., 2012). Future work could include the construction of a strain with a fluorescent marker on actin that could be incorporated into rings (e.g. through the use of unnatural amino acids). Fluorescence Recovery After Photobleaching (FRAP) could then be used to document actin dynamics in rings.

In the second part of thesis, we looked into the role of actomyosin ring in division of protoplasts from cell wall mutants. As turgor pressure exists in cells to maintain cell shape, it is likely to oppose membrane invagination during actomyosin ring contraction. *cps1* mutant (β-glucan synthase mutant) is unable to undergo actomyosin ring contraction in both normal and lowered turgor pressure. However, when the cell wall is weakened (in a protoplast) and cell wall regeneration is inhibited, the actomyosin ring contracted, resulting in cell membrane invagination and eventually cytofission. Though the protoplasts underwent cytofission, the rate of ring contraction is compromised, and in some cases the actomyosin ring disassembled before complete cell separation. Through electron microscopy, we observed significantly less cell wall surrounding

the protoplast, reinforcing our presumption that actomyosin ring is capable to drive cell membrane invagination when cell wall is weakened. The divided protoplasts are capable of normal nuclear distribution between daughter cells, while a portion behaved abnormally and contained two nuclei and / or cleaved nuclei during cell separation.

Since cell wall is composed of β-glucan and α-glucan, we generated double mutant protoplast defective in synthesizing β-glucan and α-glucan. We found that actomyosin ring is still able to contract in these protoplasts. Given that cell wall is dispensable in the cytofission of *cps1* mutant protoplast, we also found that this process does not require break-down of cell wall materials by exoglucanases. Likewise, *cps1* mutant protoplast does not require ESCRT proteins Vps20 and Vps4 to undergo cytofission. We showed that actin and myosin are essential for the actomyosin ring contraction in the case of protoplasts. Both Latrunculin A treatment and deletion of myosin regulatory light chain *rlc1* impeded actomyosin ring contraction and cell separation. Furthermore, our results indicate that membrane trafficking coupled with actomyosin ring contraction is essential for cytofission events.

As the actomyosin ring disassembled when the protoplast is undergoing cytofission, we would expect the several outcomes due to the loss of force around the invaginated membrane. For instance, smaller entity of the dividing protoplast retract to the larger entity, or restoration of protoplast to a sphere, losing its dumbbell appearance. Question that remained to be answered will be what are the factors driving the membrane invagination to cell separation after disassembly of actomyosin ring.

6. BIBLIOGRAPHY

1. Wu, J.Q. and T.D. Pollard, *Counting cytokinesis proteins globally and locally in fission yeast.* Science, 2005. **310**(5746): p. 310-4.
2. Pollard, T.D. and J.Q. Wu, *Understanding cytokinesis: lessons from fission yeast.* Nat Rev Mol Cell Biol, 2010. **11**(2): p. 149-55.
3. Lutkenhaus, J. and S.G. Addinall, *Bacterial cell division and the Z ring.* Annu Rev Biochem, 1997. **66**: p. 93-116.
4. Bi, E.F. and J. Lutkenhaus, *FtsZ ring structure associated with division in Escherichia coli.* Nature, 1991. **354**(6349): p. 161-4.
5. Errington, J., R.A. Daniel, and D.J. Scheffers, *Cytokinesis in bacteria.* Microbiol Mol Biol Rev, 2003. **67**(1): p. 52-65, table of contents.
6. Levin, P.A. and R. Losick, *Transcription factor Spo0A switches the localization of the cell division protein FtsZ from a medial to a bipolar pattern in Bacillus subtilis.* Genes Dev, 1996. **10**(4): p. 478-88.
7. Addinall, S.G., E. Bi, and J. Lutkenhaus, *FtsZ ring formation in fts mutants.* J Bacteriol, 1996. **178**(13): p. 3877-84.
8. de Boer, P., R. Crossley, and L. Rothfield, *The essential bacterial cell-division protein FtsZ is a GTPase.* Nature, 1992. **359**(6392): p. 254-6.
9. Mukherjee, A. and J. Lutkenhaus, *Guanine nucleotide-dependent assembly of FtsZ into filaments.* J Bacteriol, 1994. **176**(9): p. 2754-8.
10. RayChaudhuri, D. and J.T. Park, *A point mutation converts Escherichia coli FtsZ septation GTPase to an ATPase.* J Biol Chem, 1994. **269**(37): p. 22941-4.

11. Busiek, K.K. and W. Margolin, *Bacterial actin and tubulin homologs in cell growth and division.* Curr Biol, 2015. **25**(6): p. R243-R254.
12. van den Ent, F. and J. Lowe, *Crystal structure of the cell division protein FtsA from Thermotoga maritima.* EMBO J, 2000. **19**(20): p. 5300-7.
13. van den Ent, F., L.A. Amos, and J. Lowe, *Prokaryotic origin of the actin cytoskeleton.* Nature, 2001. **413**(6851): p. 39-44.
14. Addinall, S.G. and J. Lutkenhaus, *FtsA is localized to the septum in an FtsZ-dependent manner.* J Bacteriol, 1996. **178**(24): p. 7167-72.
15. Rico, A.I., et al., *Role of two essential domains of Escherichia coli FtsA in localization and progression of the division ring.* Mol Microbiol, 2004. **53**(5): p. 1359-71.
16. Slovak, P.M., G.H. Wadhams, and J.P. Armitage, *Localization of MreB in Rhodobacter sphaeroides under conditions causing changes in cell shape and membrane structure.* J Bacteriol, 2005. **187**(1): p. 54-64.
17. Fenton, A.K. and K. Gerdes, *Direct interaction of FtsZ and MreB is required for septum synthesis and cell division in Escherichia coli.* EMBO J, 2013. **32**(13): p. 1953-65.
18. Liechti, G.W., et al., *A new metabolic cell-wall labelling method reveals peptidoglycan in Chlamydia trachomatis.* Nature, 2014. **506**(7489): p. 507-10.
19. Pilhofer, M., et al., *Discovery of chlamydial peptidoglycan reveals bacteria with murein sacculi but without FtsZ.* Nat Commun, 2013. **4**: p. 2856.
20. Woldringh, C.L., et al., *Toporegulation of bacterial division according to the nucleoid occlusion model.* Res Microbiol, 1991. **142**(2-3): p. 309-20.

21. de Boer, P.A., R.E. Crossley, and L.I. Rothfield, *Roles of MinC and MinD in the site-specific septation block mediated by the MinCDE system of Escherichia coli.* J Bacteriol, 1992. **174**(1): p. 63-70.
22. van Baarle, S. and M. Bramkamp, *The MinCDJ system in Bacillus subtilis prevents minicell formation by promoting divisome disassembly.* PLoS One, 2010. **5**(3): p. e9850.
23. Gregory, J.A., E.C. Becker, and K. Pogliano, *Bacillus subtilis MinC destabilizes FtsZ-rings at new cell poles and contributes to the timing of cell division.* Genes Dev, 2008. **22**(24): p. 3475-88.
24. Addinall, S.G. and J. Lutkenhaus, *FtsZ-spirals and -arcs determine the shape of the invaginating septa in some mutants of Escherichia coli.* Mol Microbiol, 1996. **22**(2): p. 231-7.
25. Carvalho, A., A. Desai, and K. Oegema, *Structural memory in the contractile ring makes the duration of cytokinesis independent of cell size.* Cell, 2009. **137**(5): p. 926-37.
26. Khaliullin, R.N., et al., *A positive-feedback-based mechanism for constriction rate acceleration during cytokinesis in Caenorhabditis elegans.* Elife, 2018. **7**.
27. Allard, J.F. and E.N. Cytrynbaum, *Force generation by a dynamic Z-ring in Escherichia coli cell division.* Proc Natl Acad Sci U S A, 2009. **106**(1): p. 145-50.
28. Mukherjee, A. and J. Lutkenhaus, *Dynamic assembly of FtsZ regulated by GTP hydrolysis.* EMBO J, 1998. **17**(2): p. 462-9.
29. Lu, C., M. Reedy, and H.P. Erickson, *Straight and curved conformations of FtsZ are regulated by GTP hydrolysis.* J Bacteriol, 2000. **182**(1): p. 164-70.
30. Osawa, M., D.E. Anderson, and H.P. Erickson, *Curved FtsZ protofilaments generate bending forces on liposome membranes.* EMBO J, 2009. **28**(22): p. 3476-84.

31. Watanabe, S., et al., *mDia2 induces the actin scaffold for the contractile ring and stabilizes its position during cytokinesis in NIH 3T3 cells.* Mol Biol Cell, 2008. **19**(5): p. 2328-38.
32. Madaule, P., et al., *Role of citron kinase as a target of the small GTPase Rho in cytokinesis.* Nature, 1998. **394**(6692): p. 491-4.
33. Kosako, H., et al., *Rho-kinase/ROCK is involved in cytokinesis through the phosphorylation of myosin light chain and not ezrin/radixin/moesin proteins at the cleavage furrow.* Oncogene, 2000. **19**(52): p. 6059-64.
34. Ueda, K., et al., *Rho-kinase contributes to diphosphorylation of myosin II regulatory light chain in nonmuscle cells.* Oncogene, 2002. **21**(38): p. 5852-60.
35. Yamashiro, S., et al., *Citron kinase, a Rho-dependent kinase, induces di-phosphorylation of regulatory light chain of myosin II.* Mol Biol Cell, 2003. **14**(5): p. 1745-56.
36. Piekny, A., M. Werner, and M. Glotzer, *Cytokinesis: welcome to the Rho zone.* Trends Cell Biol, 2005. **15**(12): p. 651-8.
37. Werner, M., E. Munro, and M. Glotzer, *Astral signals spatially bias cortical myosin recruitment to break symmetry and promote cytokinesis.* Curr Biol, 2007. **17**(15): p. 1286-97.
38. Trotter, J.A. and R.S. Adelstein, *Macrophage myosin. Regulation of actin-activated ATPase, activity by phosphorylation of the 20,000-dalton light chain.* J Biol Chem, 1979. **254**(18): p. 8781-5.
39. Mabuchi, I. and M. Okuno, *The effect of myosin antibody on the division of starfish blastomeres.* J Cell Biol, 1977. **74**(1): p. 251-63.
40. Guo, S. and K.J. Kemphues, *A non-muscle myosin required for embryonic polarity in Caenorhabditis elegans.* Nature, 1996. **382**(6590): p. 455-8.

41. Karess, R.E., et al., *The regulatory light chain of nonmuscle myosin is encoded by spaghetti-squash, a gene required for cytokinesis in Drosophila.* Cell, 1991. **65**(7): p. 1177-89.
42. Shelton, C.A., et al., *The nonmuscle myosin regulatory light chain gene mlc-4 is required for cytokinesis, anterior-posterior polarity, and body morphology during Caenorhabditis elegans embryogenesis.* J Cell Biol, 1999. **146**(2): p. 439-51.
43. Young, P.E., et al., *Morphogenesis in Drosophila requires nonmuscle myosin heavy chain function.* Genes Dev, 1993. **7**(1): p. 29-41.
44. Celton-Morizur, S., et al., *C-terminal anchoring of mid1p to membranes stabilizes cytokinetic ring position in early mitosis in fission yeast.* Mol Cell Biol, 2004. **24**(24): p. 10621-35.
45. Lacroix, B. and A.S. Maddox, *Cytokinesis, ploidy and aneuploidy.* J Pathol, 2012. **226**(2): p. 338-51.
46. Strauss, B., R.J. Adams, and N. Papalopulu, *A default mechanism of spindle orientation based on cell shape is sufficient to generate cell fate diversity in polarised Xenopus blastomeres.* Development, 2006. **133**(19): p. 3883-93.
47. D'Avino, P.P., M.G. Giansanti, and M. Petronczki, *Cytokinesis in animal cells.* Cold Spring Harb Perspect Biol, 2015. **7**(4): p. a015834.
48. Fededa, J.P. and D.W. Gerlich, *Molecular control of animal cell cytokinesis.* Nat Cell Biol, 2012. **14**(5): p. 440-7.
49. Jordan, S.N. and J.C. Canman, *Rho GTPases in animal cell cytokinesis: an occupation by the one percent.* Cytoskeleton (Hoboken), 2012. **69**(11): p. 919-30.
50. Bement, W.M., H.A. Benink, and G. von Dassow, *A microtubule-dependent zone of active RhoA during cleavage plane specification.* J Cell Biol, 2005. **170**(1): p. 91-101.

51. Schmutz, C., J. Stevens, and A. Spang, *Functions of the novel RhoGAP proteins RGA-3 and RGA-4 in the germ line and in the early embryo of C. elegans.* Development, 2007. **134**(19): p. 3495-505.
52. Schonegg, S., et al., *The Rho GTPase-activating proteins RGA-3 and RGA-4 are required to set the initial size of PAR domains in Caenorhabditis elegans one-cell embryos.* Proc Natl Acad Sci U S A, 2007. **104**(38): p. 14976-81.
53. Zanin, E., et al., *A conserved RhoGAP limits M phase contractility and coordinates with microtubule asters to confine RhoA during cytokinesis.* Dev Cell, 2013. **26**(5): p. 496-510.
54. Motegi, F., et al., *Two phases of astral microtubule activity during cytokinesis in C. elegans embryos.* Dev Cell, 2006. **10**(4): p. 509-20.
55. Toya, M., et al., *A kinase-independent role for Aurora A in the assembly of mitotic spindle microtubules in Caenorhabditis elegans embryos.* Nat Cell Biol, 2011. **13**(6): p. 708-14.
56. Ozlu, N., et al., *An essential function of the C. elegans ortholog of TPX2 is to localize activated aurora A kinase to mitotic spindles.* Dev Cell, 2005. **9**(2): p. 237-48.
57. Mangal, S., et al., *TPXL-1 activates Aurora A to clear contractile ring components from the polar cortex during cytokinesis.* J Cell Biol, 2018. **217**(3): p. 837-848.
58. Pollard, T.D. and B. O'Shaughnessy, *Molecular Mechanism of Cytokinesis.* Annu Rev Biochem, 2019. **88**: p. 661-689.
59. Bose, I., et al., *Assembly of scaffold-mediated complexes containing Cdc42p, the exchange factor Cdc24p, and the effector Cla4p required for cell cycle-regulated phosphorylation of Cdc24p.* J Biol Chem, 2001. **276**(10): p. 7176-86.

60. Butty, A.C., et al., *A positive feedback loop stabilizes the guanine-nucleotide exchange factor Cdc24 at sites of polarization.* EMBO J, 2002. **21**(7): p. 1565-76.
61. Endo, M., M. Shirouzu, and S. Yokoyama, *The Cdc42 binding and scaffolding activities of the fission yeast adaptor protein Scd2.* J Biol Chem, 2003. **278**(2): p. 843-52.
62. Irazoqui, J.E., A.S. Gladfelter, and D.J. Lew, *Scaffold-mediated symmetry breaking by Cdc42p.* Nat Cell Biol, 2003. **5**(12): p. 1062-70.
63. Ito, T., et al., *Novel modular domain PB1 recognizes PC motif to mediate functional protein-protein interactions.* EMBO J, 2001. **20**(15): p. 3938-46.
64. Kozubowski, L., et al., *Symmetry-breaking polarization driven by a Cdc42p GEF-PAK complex.* Curr Biol, 2008. **18**(22): p. 1719-26.
65. Bertin, A., et al., *Saccharomyces cerevisiae septins: supramolecular organization of heterooligomers and the mechanism of filament assembly.* Proc Natl Acad Sci U S A, 2008. **105**(24): p. 8274-9.
66. Garcia, G., 3rd, et al., *Subunit-dependent modulation of septin assembly: budding yeast septin Shs1 promotes ring and gauze formation.* J Cell Biol, 2011. **195**(6): p. 993-1004.
67. Iwase, M., et al., *Role of a Cdc42p effector pathway in recruitment of the yeast septins to the presumptive bud site.* Mol Biol Cell, 2006. **17**(3): p. 1110-25.
68. Wloka, C. and E. Bi, *Mechanisms of cytokinesis in budding yeast.* Cytoskeleton (Hoboken), 2012. **69**(10): p. 710-26.
69. Bi, E., et al., *Involvement of an actomyosin contractile ring in Saccharomyces cerevisiae cytokinesis.* J Cell Biol, 1998. **142**(5): p. 1301-12.

70. Lippincott, J. and R. Li, *Sequential assembly of myosin II, an IQGAP-like protein, and filamentous actin to a ring structure involved in budding yeast cytokinesis.* J Cell Biol, 1998. **140**(2): p. 355-66.
71. Almonacid, M., et al., *Spatial control of cytokinesis by Cdr2 kinase and Mid1/anillin nuclear export.* Curr Biol, 2009. **19**(11): p. 961-6.
72. Moseley, J.B., et al., *A spatial gradient coordinates cell size and mitotic entry in fission yeast.* Nature, 2009. **459**(7248): p. 857-60.
73. Sohrmann, M., et al., *The dmf1/mid1 gene is essential for correct positioning of the division septum in fission yeast.* Genes Dev, 1996. **10**(21): p. 2707-19.
74. Tran, P.T., et al., *A mechanism for nuclear positioning in fission yeast based on microtubule pushing.* J Cell Biol, 2001. **153**(2): p. 397-411.
75. Daga, R.R. and F. Chang, *Dynamic positioning of the fission yeast cell division plane.* Proc Natl Acad Sci U S A, 2005. **102**(23): p. 8228-32.
76. Tolic-Norrelykke, I.M., et al., *Nuclear and division-plane positioning revealed by optical micromanipulation.* Curr Biol, 2005. **15**(13): p. 1212-6.
77. Morrell, J.L., C.B. Nichols, and K.L. Gould, *The GIN4 family kinase, Cdr2p, acts independently of septins in fission yeast.* J Cell Sci, 2004. **117**(Pt 22): p. 5293-302.
78. Rincon, S.A., et al., *Pom1 regulates the assembly of Cdr2-Mid1 cortical nodes for robust spatial control of cytokinesis.* J Cell Biol, 2014. **206**(1): p. 61-77.
79. Padte, N.N., et al., *The cell-end factor pom1p inhibits mid1p in specification of the cell division plane in fission yeast.* Curr Biol, 2006. **16**(24): p. 2480-7.

80. Bahler, J., et al., *Role of polo kinase and Mid1p in determining the site of cell division in fission yeast.* J Cell Biol, 1998. **143**(6): p. 1603-16.
81. Huang, Y., et al., *Polarity determinants Tea1p, Tea4p, and Pom1p inhibit division-septum assembly at cell ends in fission yeast.* Dev Cell, 2007. **12**(6): p. 987-96.
82. Chang, F., D. Drubin, and P. Nurse, *cdc12p, a protein required for cytokinesis in fission yeast, is a component of the cell division ring and interacts with profilin.* J Cell Biol, 1997. **137**(1): p. 169-82.
83. Wu, J.Q., et al., *Assembly of the cytokinetic contractile ring from a broad band of nodes in fission yeast.* J Cell Biol, 2006. **174**(3): p. 391-402.
84. Schaller, M.D., *Paxillin: a focal adhesion-associated adaptor protein.* Oncogene, 2001. **20**(44): p. 6459-72.
85. Arasada, R. and T.D. Pollard, *Contractile ring stability in S. pombe depends on F-BAR protein Cdc15p and Bgs1p transport from the Golgi complex.* Cell Rep, 2014. **8**(5): p. 1533-44.
86. Guzman-Vendrell, M., et al., *Molecular control of the Wee1 regulatory pathway by the SAD kinase Cdr2.* J Cell Sci, 2015. **128**(15): p. 2842-53.
87. Goss, J.W., et al., *Characterization of the roles of Blt1p in fission yeast cytokinesis.* Mol Biol Cell, 2014. **25**(13): p. 1946-57.
88. Guzman-Vendrell, M., et al., *Blt1 and Mid1 provide overlapping membrane anchors to position the division plane in fission yeast.* Mol Cell Biol, 2013. **33**(2): p. 418-28.
89. Akamatsu, M., et al., *Cytokinetic nodes in fission yeast arise from two distinct types of nodes that merge during interphase.* J Cell Biol, 2014. **204**(6): p. 977-88.

90. Vavylonis, D., et al., *Assembly mechanism of the contractile ring for cytokinesis by fission yeast.* Science, 2008. **319**(5859): p. 97-100.
91. Marks, J., and J.S. Hyams, *Localization of F-actin through the cell division cycle of Schizosaccharomyces pombe.* Eur. J. Cell Biol, 1985. **39**: p. 27-32.
92. Glynn, J.M., et al., *Role of bud6p and tea1p in the interaction between actin and microtubules for the establishment of cell polarity in fission yeast.* Curr Biol, 2001. **11**(11): p. 836-45.
93. Drake, T., E. Yusuf, and D. Vavylonis, *A systems-biology approach to yeast actin cables.* Adv Exp Med Biol, 2012. **736**: p. 325-35.
94. Moseley, J.B. and B.L. Goode, *The yeast actin cytoskeleton: from cellular function to biochemical mechanism.* Microbiol Mol Biol Rev, 2006. **70**(3): p. 605-45.
95. Kovar, D.R., V. Sirotkin, and M. Lord, *Three's company: the fission yeast actin cytoskeleton.* Trends Cell Biol, 2011. **21**(3): p. 177-87.
96. Arai, R., K. Nakano, and I. Mabuchi, *Subcellular localization and possible function of actin, tropomyosin and actin-related protein 3 (Arp3) in the fission yeast Schizosaccharomyces pombe.* Eur J Cell Biol, 1998. **76**(4): p. 288-95.
97. Arai, R. and I. Mabuchi, *F-actin ring formation and the role of F-actin cables in the fission yeast Schizosaccharomyces pombe.* J Cell Sci, 2002. **115**(Pt 5): p. 887-98.
98. Kamasaki, T., et al., *Directionality of F-actin cables changes during the fission yeast cell cycle.* Nat Cell Biol, 2005. **7**(9): p. 916-7.
99. Fujime, S., *Quasi-elastic light scattering from solutions of macromolecules. II. Doppler broadening of light scattered from*

solutions of semi-flexible polymers, Factin. . J. Phys. Soc. Jpn, 1970. **29**: p. 751-759.

100. Fujime, S. and S. Ishiwata, *Dynamic study of F-actin by quasielastic scattering of laser light.* J Mol Biol, 1971. **62**(1): p. 251-65.
101. Gittes, F., et al., *Flexural rigidity of microtubules and actin filaments measured from thermal fluctuations in shape.* J Cell Biol, 1993. **120**(4): p. 923-34.
102. Isambert, H., et al., *Flexibility of actin filaments derived from thermal fluctuations. Effect of bound nucleotide, phalloidin, and muscle regulatory proteins.* J Biol Chem, 1995. **270**(19): p. 11437-44.
103. M.S. e Silva, J.A., J. Nguyen, N. Georgoulia, B.M. Mulder, G.H. Koenderink, *Self-organized patterns of actin filaments in cell-sized confinement.* Soft Matter, 2011. **7**: p. 10631-10641.
104. Coffman, V.C., et al., *Roles of formin nodes and myosin motor activity in Mid1p-dependent contractile-ring assembly during fission yeast cytokinesis.* Mol Biol Cell, 2009. **20**(24): p. 5195-210.
105. Wu, J.Q., J. Bahler, and J.R. Pringle, *Roles of a fimbrin and an alpha-actinin-like protein in fission yeast cell polarization and cytokinesis.* Mol Biol Cell, 2001. **12**(4): p. 1061-77.
106. Laporte, D., R. Zhao, and J.Q. Wu, *Mechanisms of contractile-ring assembly in fission yeast and beyond.* Semin Cell Dev Biol, 2010. **21**(9): p. 892-8.
107. Wu, J.Q., et al., *Spatial and temporal pathway for assembly and constriction of the contractile ring in fission yeast cytokinesis.* Dev Cell, 2003. **5**(5): p. 723-34.
108. Hachet, O. and V. Simanis, *Mid1p/anillin and the septation initiation network orchestrate contractile ring assembly for cytokinesis.* Genes Dev, 2008. **22**(22): p. 3205-16.

109. Huang, Y., H. Yan, and M.K. Balasubramanian, *Assembly of normal actomyosin rings in the absence of Mid1p and cortical nodes in fission yeast.* J Cell Biol, 2008. **183**(6): p. 979-88.
110. Mishra, M., et al., *The Clp1p/Flp1p phosphatase ensures completion of cytokinesis in response to minor perturbation of the cell division machinery in Schizosaccharomyces pombe.* J Cell Sci, 2004. **117**(Pt 17): p. 3897-910.
111. Dey, S.K. and T.D. Pollard, *Involvement of the septation initiation network in events during cytokinesis in fission yeast.* J Cell Sci, 2018. **131**(16).
112. Zambon, P., et al., *Myo2p is the major motor involved in actomyosin ring contraction in fission yeast.* Curr Biol, 2017. **27**(3): p. R99-R100.
113. Palani, S., et al., *Motor Activity Dependent and Independent Functions of Myosin II Contribute to Actomyosin Ring Assembly and Contraction in Schizosaccharomyces pombe.* Curr Biol, 2017. **27**(5): p. 751-757.
114. Kitayama, C., A. Sugimoto, and M. Yamamoto, *Type II myosin heavy chain encoded by the myo2 gene composes the contractile ring during cytokinesis in Schizosaccharomyces pombe.* J Cell Biol, 1997. **137**(6): p. 1309-19.
115. Guha, M., M. Zhou, and Y.L. Wang, *Cortical actin turnover during cytokinesis requires myosin II.* Curr Biol, 2005. **15**(8): p. 732-6.
116. Fujiwara, K. and T.D. Pollard, *Fluorescent antibody localization of myosin in the cytoplasm, cleavage furrow, and mitotic spindle of human cells.* J Cell Biol, 1976. **71**(3): p. 848-75.
117. Oelz, D.B., B.Y. Rubinstein, and A. Mogilner, *A Combination of Actin Treadmilling and Cross-Linking Drives Contraction of Random Actomyosin Arrays.* Biophys J, 2015. **109**(9): p. 1818-29.

118. Schmidt, O. and D. Teis, *The ESCRT machinery.* Curr Biol, 2012. **22**(4): p. R116-20.
119. Mierzwa, B. and D.W. Gerlich, *Cytokinetic abscission: molecular mechanisms and temporal control.* Dev Cell, 2014. **31**(5): p. 525-38.
120. Henne, W.M., H. Stenmark, and S.D. Emr, *Molecular mechanisms of the membrane sculpting ESCRT pathway.* Cold Spring Harb Perspect Biol, 2013. **5**(9).
121. Peel, S., et al., *Divergent pathways lead to ESCRT-III-catalyzed membrane fission.* Trends Biochem Sci, 2011. **36**(4): p. 199-210.
122. Kopecka, M., G.H. Fleet, and H.J. Phaff, *Ultrastructure of the cell wall of Schizosaccharomyces pombe following treatment with various glucanases.* J Struct Biol, 1995. **114**(2): p. 140-52.
123. David J.Manners, M.T.M., *The molecular structures of some glucans from the cell walls of Schizosaccharomyces pombe.* Carbohydrate Research, 1977. **57**: p. 189-203.
124. Bush, D.A., et al., *The wall structure of Schizosaccharomyces pombe.* J Gen Microbiol, 1974. **81**(1): p. 199-206.
125. Liu, J., et al., *Drc1p/Cps1p, a 1,3-beta-glucan synthase subunit, is essential for division septum assembly in Schizosaccharomyces pombe.* Genetics, 1999. **153**(3): p. 1193-203.
126. Le Goff, X., A. Woollard, and V. Simanis, *Analysis of the cps1 gene provides evidence for a septation checkpoint in Schizosaccharomyces pombe.* Mol Gen Genet, 1999. **262**(1): p. 163-72.
127. Liu, J., H. Wang, and M.K. Balasubramanian, *A checkpoint that monitors cytokinesis in Schizosaccharomyces pombe.* J Cell Sci, 2000. **113 (Pt 7)**: p. 1223-30.

128. Katayama, S., et al., *Fission yeast alpha-glucan synthase Mok1 requires the actin cytoskeleton to localize the sites of growth and plays an essential role in cell morphogenesis downstream of protein kinase C function.* J Cell Biol, 1999. **144**(6): p. 1173-86.
129. Martin-Cuadrado, A.B., et al., *The Schizosaccharomyces pombe endo-1,3-beta-glucanase Eng1 contains a novel carbohydrate binding module required for septum localization.* Mol Microbiol, 2008. **69**(1): p. 188-200.
130. Dekker, N., et al., *Role of the alpha-glucanase Agn1p in fission-yeast cell separation.* Mol Biol Cell, 2004. **15**(8): p. 3903-14.
131. Martin-Cuadrado, A.B., et al., *The endo-beta-1,3-glucanase eng1p is required for dissolution of the primary septum during cell separation in Schizosaccharomyces pombe.* J Cell Sci, 2003. **116**(Pt 9): p. 1689-98.
132. Garcia, I., et al., *The alpha-glucanase Agn1p is required for cell separation in Schizosaccharomyces pombe.* Biol Cell, 2005. **97**(7): p. 569-76.
133. Huang, J., et al., *Nonmedially assembled F-actin cables incorporate into the actomyosin ring in fission yeast.* J Cell Biol, 2012. **199**(5): p. 831-47.
134. Paoletti, A. and F. Chang, *Analysis of mid1p, a protein required for placement of the cell division site, reveals a link between the nucleus and the cell surface in fission yeast.* Mol Biol Cell, 2000. **11**(8): p. 2757-73.
135. Chang, F., A. Woollard, and P. Nurse, *Isolation and characterization of fission yeast mutants defective in the assembly and placement of the contractile actin ring.* J Cell Sci, 1996. **109 (Pt 1)**: p. 131-42.

136. Fankhauser, C., et al., *The S. pombe cdc15 gene is a key element in the reorganization of F-actin at mitosis.* Cell, 1995. **82**(3): p. 435-44.
137. Carnahan, R.H. and K.L. Gould, *The PCH family protein, Cdc15p, recruits two F-actin nucleation pathways to coordinate cytokinetic actin ring formation in Schizosaccharomyces pombe.* J Cell Biol, 2003. **162**(5): p. 851-62.
138. Rincon, S.A. and A. Paoletti, *Molecular control of fission yeast cytokinesis.* Semin Cell Dev Biol, 2016. **53**: p. 28-38.
139. Mishra, M., et al., *Cylindrical cellular geometry ensures fidelity of division site placement in fission yeast.* J Cell Sci, 2012. **125**(Pt 16): p. 3850-7.
140. Ge, W., et al., *The novel fission yeast protein Pal1p interacts with Hip1-related Sla2p/End4p and is involved in cellular morphogenesis.* Mol Biol Cell, 2005. **16**(9): p. 4124-38.
141. Sipiczki, M., et al., *Role of cell shape in determination of the division plane in Schizosaccharomyces pombe: random orientation of septa in spherical cells.* J Bacteriol, 2000. **182**(6): p. 1693-701.
142. Munoz, J., et al., *Extracellular cell wall beta(1,3)glucan is required to couple septation to actomyosin ring contraction.* J Cell Biol, 2013. **203**(2): p. 265-82.
143. Willet, A.H., et al., *The F-BAR Cdc15 promotes contractile ring formation through the direct recruitment of the formin Cdc12.* J Cell Biol, 2015. **208**(4): p. 391-9.
144. Balasubramanian, M.K., et al., *The Schizosaccharomyces pombe cdc3+ gene encodes a profilin essential for cytokinesis.* J Cell Biol, 1994. **125**(6): p. 1289-301.

145. Suarez, C., et al., *Profilin regulates F-actin network homeostasis by favoring formin over Arp2/3 complex.* Dev Cell, 2015. **32**(1): p. 43-53.
146. Marina Soares e Silva, J.A., Jeanette Nguyen, Nefeli Georgoulia, Bela M. Muldera and Gijsje H. Koenderink, *Self-organized patterns of actin filaments in cell-sized confinement.* Soft Matter, 2011. **7**(22): p. 10631-10641.
147. M. M. A. E. Claessens, R.T., K. Kroy and A. R. Bausch, *Microstructure and viscoelasticity of confined semiflexible polymer networks.* Nature Physics, 2006. **2**: p. 186-189.
148. Riveline, D., Wiggins, C.H., Goldstein, R.E., and Ott, A., *Elastohydrodynamic study of actin filaments using fluorescence microscopy.* Phys. Rev. E 56 R1330, 1997.
149. Courtemanche, N., T.D. Pollard, and Q. Chen, *Avoiding artefacts when counting polymerized actin in live cells with LifeAct fused to fluorescent proteins.* Nat Cell Biol, 2016. **18**(6): p. 676-83.
150. Kamasaki, T., M. Osumi, and I. Mabuchi, *Three-dimensional arrangement of F-actin in the contractile ring of fission yeast.* J Cell Biol, 2007. **178**(5): p. 765-71.
151. Laporte, D., et al., *Assembly and architecture of precursor nodes during fission yeast cytokinesis.* J Cell Biol, 2011. **192**(6): p. 1005-21.
152. Hochstenbach, F., et al., *Identification of a putative alpha-glucan synthase essential for cell wall construction and morphogenesis in fission yeast.* Proc Natl Acad Sci U S A, 1998. **95**(16): p. 9161-6.
153. Klis, F.M., et al., *Dynamics of cell wall structure in Saccharomyces cerevisiae.* FEMS Microbiol Rev, 2002. **26**(3): p. 239-56.

154. Garcia Cortes, J.C., et al., *The Cell Biology of Fission Yeast Septation.* Microbiol Mol Biol Rev, 2016. **80**(3): p. 779-91.
155. Chang, F., *Studies in fission yeast on mechanisms of cell division site placement.* Cell Struct Funct, 2001. **26**(6): p. 539-44.
156. McCollum, D. and K.L. Gould, *Timing is everything: regulation of mitotic exit and cytokinesis by the MEN and SIN.* Trends Cell Biol, 2001. **11**(2): p. 89-95.
157. Elia, N., et al., *Dynamics of endosomal sorting complex required for transport (ESCRT) machinery during cytokinesis and its role in abscission.* Proc Natl Acad Sci U S A, 2011. **108**(12): p. 4846-51.
158. Elia, N., et al., *Computational model of cytokinetic abscission driven by ESCRT-III polymerization and remodeling.* Biophys J, 2012. **102**(10): p. 2309-20.
159. Lata, S., et al., *Helical structures of ESCRT-III are disassembled by VPS4.* Science, 2008. **321**(5894): p. 1354-7.
160. Morita, E., et al., *Human ESCRT and ALIX proteins interact with proteins of the midbody and function in cytokinesis.* EMBO J, 2007. **26**(19): p. 4215-27.
161. Saksena, S., et al., *ESCRTing proteins in the endocytic pathway.* Trends Biochem Sci, 2007. **32**(12): p. 561-73.
162. Sipiczki, M., *Splitting of the fission yeast septum.* FEMS Yeast Res, 2007. **7**(6): p. 761-70.
163. Moreno, S., A. Klar, and P. Nurse, *Molecular genetic analysis of fission yeast Schizosaccharomyces pombe.* Methods Enzymol, 1991. **194**: p. 795-823.
164. E.F. Gale, F.W., P.A. Orlean, *The Action of 2-Deoxyglucose on the Incorporation of Glucose into (1-3)-beta-Glucan in Stationary Phase Cultures of Candida albicans.* Journal of General Microbiology, 1984. **130**.

165. Proctor, S.A., et al., *Contributions of turgor pressure, the contractile ring, and septum assembly to forces in cytokinesis in fission yeast.* Curr Biol, 2012. **22**(17): p. 1601-8.
166. Flor-Parra, I., et al., *Cell migration and division in amoeboid-like fission yeast.* Biol Open, 2014. **3**(1): p. 108-15.
167. Choudhary, A., et al., *Interphase cytofission maintains genomic integrity of human cells after failed cytokinesis.* Proc Natl Acad Sci U S A, 2013. **110**(32): p. 13026-31.
168. Fujiwara, I., et al., *Latrunculin A Accelerates Actin Filament Depolymerization in Addition to Sequestering Actin Monomers.* Curr Biol, 2018. **28**(19): p. 3183-3192 e2.
169. Morton, W.M., K.R. Ayscough, and P.J. McLaughlin, *Latrunculin alters the actin-monomer subunit interface to prevent polymerization.* Nat Cell Biol, 2000. **2**(6): p. 376-8.
170. Naqvi, N.I., et al., *Type II myosin regulatory light chain relieves auto-inhibition of myosin-heavy-chain function.* Nat Cell Biol, 2000. **2**(11): p. 855-8.
171. Le Goff, X., et al., *The S. pombe rlc1 gene encodes a putative myosin regulatory light chain that binds the type II myosins myo3p and myo2p.* J Cell Sci, 2000. **113 Pt 23**: p. 4157-63.
172. Pollard, L.W., et al., *Fission yeast myosin Myo2 is down-regulated in actin affinity by light chain phosphorylation.* Proc Natl Acad Sci U S A, 2017. **114**(35): p. E7236-E7244.
173. Basu, R., E.L. Munteanu, and F. Chang, *Role of turgor pressure in endocytosis in fission yeast.* Mol Biol Cell, 2014. **25**(5): p. 679-87.
174. Levin, D.E. and E. Bartlett-Heubusch, *Mutants in the S. cerevisiae PKC1 gene display a cell cycle-specific osmotic stability defect.* J Cell Biol, 1992. **116**(5): p. 1221-9.

175. Jochova, J., I. Rupes, and E. Streiblova, *F-actin contractile rings in protoplasts of the yeast Schizosaccharomyces.* Cell Biol Int Rep, 1991. **15**(7): p. 607-10.
176. Stachowiak, M.R., et al., *Mechanism of cytokinetic contractile ring constriction in fission yeast.* Dev Cell, 2014. **29**(5): p. 547-561.